Article

Cold memories control whole-body thermoregulatory responses

https://doi.org/10.1038/s41586-025-08902-6

Received: 16 February 2024

Accepted: 14 March 2025

Published online: 23 April 2025

Open access

Check for updates

Andrea Muñoz Zamora[1,2,13], Aaron Douglas[1,2,13], Paul B. Conway[1,2], Esteban Urrieta[1,2], Taylor Moniz[1,2,3], James D. O'Leary[1,2], Lydia Marks[1,2,4], Christine A. Denny[3,5,6], Clara Ortega-de San Luis[1,2,7], Lydia Lynch[1,8,9,10] & Tomás J. Ryan[1,2,11,12] ✉

Environmental thermal challenges trigger the brain to coordinate both autonomic and behavioural responses to maintain optimal body temperature[1–4]. It is unknown how temperature information is precisely stored and retrieved in the brain and how it is converted into a physiological response. Here we investigated whether memories could control whole-body metabolism by training mice to remember a thermal challenge. Mice were conditioned to associate a context with a specific temperature by combining thermoregulatory Pavlovian conditioning with engram-labelling technology, optogenetics and chemogenetics. We report that if mice are returned to an environment in which they previously experienced a 4 °C cold challenge, they increase their metabolic rates regardless of the actual environmental temperature. Furthermore, we show that mice have increased hypothalamic activity when they are exposed to the cold, and that a specific network emerges between the hippocampus and the hypothalamus during the recall of a cold memory. Both natural retrieval and artificial reactivation of cold-sensitive memory engrams in the hippocampus mimic the physiological responses that are seen during a cold challenge. These ensembles are necessary for cold-memory retrieval. These findings show that retrieval of a cold memory causes whole-body autonomic and behavioural responses that enable mice to maintain thermal homeostasis.

The brain and the body are intrinsically connected and interact bidirectionally to maintain homeostasis[5]. Although brain–body interactions are now a central topic in neuroscience, only recently have studies shown that mental states can directly influence bodily function and that associative learning processes can modify peripheral immune and neuroendocrine responses[6–10]. However, to our knowledge, a direct link between the memory of an experience and immediate physiological changes in the body for host adaptability has yet to be identified. Here we investigated whether memories can control whole-body metabolism by training mice to remember a cold experience.

When faced with an environmental thermal challenge, birds and mammals actively maintain their body temperature in a narrow range to preserve critical cellular functions[2]. To achieve this, the brain triggers several thermoregulatory behavioural responses that maintain homeostatic body temperature—including motivated goal-directed behavioural responses such as moving to a warm place, nest building and postural changes—as well as autonomic physiological mechanisms, such as shivering, vasoconstriction and non-shivering thermogenesis[1]. The neurally regulated metabolic process of non-shivering thermogenesis contributes to the production of heat and the maintenance of core body temperature and is largely influenced by altered metabolism in brown adipose tissue (BAT)[11].

Many brain regions and neural pathways have been implicated in real-time thermoregulation, including the lateral hypothalamus (LHA), the medial preoptic area (MPO) and the xiphoid nucleus[3,4,12,13]. However, it is currently unclear whether temperature information can be stored in the brain in the form of memories. Such learned information could enable animals to anticipate thermal challenges on the basis of previous experience and allow them to respond in an energy-efficient manner. This would also require the storage, retrieval and conversion of temperature information into physiological responses. Here we investigate whether temperature information can be stored in the brain in the form of temperature-sensitive memory engrams.

The enduring physical change in the brain that accounts for a specific memory can be referred to as an engram[14]. Engram cells can be operationally defined as neuronal ensembles that are activated by learning and undergo physical changes, and the reactivation of which leads to the retrieval of the target memory[15–18]. Previous studies have identified memory engrams by combining methods that tag immediate early genes (such as *Fos* and *Arc*) with optogenetics and chemogenetics[17,19,20].

[1]School of Biochemistry and Immunology, Trinity College Dublin, Dublin, Ireland. [2]Trinity College Institute for Neuroscience, Trinity College Dublin, Dublin, Ireland. [3]Department of Psychiatry, Columbia University Irving Medical Center (CUIMC), New York, NY, USA. [4]Allen Institute, Seattle, WA, USA. [5]Division of Systems Neuroscience, Research Foundation for Mental Hygiene (RFMH), New York, NY, USA. [6]New York State Psychiatric Institute, New York, NY, USA. [7]Department of Health Sciences, University of Jaén, Jaén, Spain. [8]Brigham and Women's Hospital, Harvard Medical School, Boston, MA, USA. [9]Department of Molecular Biology, Princeton University, Princeton, NJ, USA. [10]Ludwig Cancer Research Institute, Princeton Branch, Princeton University, Princeton, NJ, USA. [11]Florey Institute of Neuroscience and Mental Health, University of Melbourne, Melbourne, Victoria, Australia. [12]Child & Brain Development Program, Canadian Institute for Advanced Research (CIFAR), Toronto, Ontario, Canada. [13]These authors contributed equally: Andrea Muñoz Zamora, Aaron Douglas. ✉e-mail: tomas.ryan@tcd.ie

By using engram-labelling technology, we investigated how temperature information is stored in the mouse brain.

We show that mice can be conditioned to associate a particular context with a cold temperature experience. A Pavlovian conditioned thermoregulatory response can thereafter be elicited by exposure to contextual stimuli associated with cold experiences. We also find that hypothalamic activity is highly upregulated when mice are exposed to the cold, and that a specific network emerges between the hippocampus and the hypothalamus during the recall of a cold memory. We show that cold-sensitive memory engrams form in the hippocampus and specific regions of the hypothalamus, and that both natural retrieval and artificial reactivation of these engrams mediate the physiological responses that are seen during a cold challenge. Furthermore, these ensembles are necessary for the retrieval of a cold memory. These results highlight that cold-sensitive engrams control whole-body autonomic and behavioural responses that enable mice to maintain thermal homeostasis.

Cold memories increase metabolism

To investigate whether mice can store and retrieve temperature information, we designed a thermoregulatory Pavlovian conditioning experiment in which mice were trained in context A at 21 °C and in context B at 4 °C (Fig. 1a,b). Cold exposure stimulates thermogenesis by increasing lipid and glucose metabolism in BAT, which in turn upregulates whole-body metabolic rate[21–23]. Mice exposed to a 4 °C environment had a lower core body temperature than when they were exposed to a 21 °C environment (Extended Data Fig. 1a–f) and showed increased oxygen consumption (Extended Data Fig. 2a), energy expenditure (Extended Data Fig. 2b) and carbon dioxide production (Extended Data Fig. 2c). Mice also moved significantly more in the 4 °C environment than in the 21 °C environment (Extended Data Fig. 2d). No differences in food consumption were observed (Extended Data Fig. 2e). We also found that the observed increase in metabolic rate and energy expenditure persisted across all three cold training days (Extended Data Fig. 2a–c). Together, these data show that mice increase their metabolic rate and alter their behaviour in response to a cold environment.

To establish whether mice can associate a specific context with a given temperature, we trained mice at 4 °C in context B and subsequently tested them in that same context at 21 °C. We observed an increase in metabolic rate when mice were returned to the cold-paired context, irrespective of the actual temperature of that context (Fig. 1c–g and Extended Data Figs. 3a,b and 4a–e). This effect was specifically induced by the contextual cues associated with cold training and not just exposure to a neutral context at baseline day 2 (BL2; Extended Data Figs. 2a–e and 4f–m). When mice were returned to the cold-paired context on test day 1 (T1), they increased their core body temperature compared with baseline day 1 (BL1; Extended Data Fig. 1b–j). Furthermore, mice showed significantly increased movement when returned to the cold-paired context (Extended Data Fig. 3c), but no difference in food consumption compared with BL1 (Extended Data Fig. 3d), suggesting that mice can adjust their behaviour in the cold-paired context on T1, similar to what is observed in the 4 °C context. Although differences in movement were found between various days, the observed increase in metabolic rate on test day was not driven solely by movement (Extended Data Fig. 4n–q). Notably, we also found a temporal dynamic on T1, as the metabolic rates resemble cold day 1 (CL1) during the first few hours and come closer to baseline levels after 6 h (Fig. 1c–g). Both male and female mice increased their metabolic rate when they were returned to the cold-paired context (Extended Data Figs. 4f–m and 5a–c).

To confirm that the upregulation of the metabolic rate on test day was due to the pairing of 4 °C and context B, and not because of the novelty of the context, we trained mice in the same Pavlovian timeline without changing the temperature from 21 °C (Fig. 1h,i). We found that, although the novelty of context B caused an increase in metabolic rate in the initial 2 h of the no-cold training and test days, there were no differences in metabolic rate between baseline, no-cold training and test after 2 h (Fig. 1j), suggesting that novelty does not affect metabolic rate after 2 h. Mice that underwent 4 °C cold training in context B were directly compared with mice that underwent the 21 °C no-cold training in context B. Our results demonstrate that cold training at 4 °C in context B significantly increased metabolic rate on T1 compared with 21 °C no-cold training (Fig. 1k). These effects are not due to initial differences between the two groups, as they did not significantly differ in metabolic rate on BL1 (Fig. 1l).

These data show that the increase in metabolic rate is not caused by the novelty of context B, but rather by the association of 4 °C with context B. To rule out the possibility that the increase in metabolic rate was due to the prolonged effects of long-term cold exposure, a separate cohort of mice was allowed to recover in their home cage for four consecutive days instead of two after cold training (Extended Data Fig. 6a–g). We found that the increase in metabolic rate persisted even after this longer recovery break, indicating that the observed increase in whole-body metabolism was not due to prolonged cold effects, but rather to the recall of the cold-paired contextual memory. To rule out the possibility that the increase in metabolic rate was due to a generalized stress response, mice were exposed to the predator odour trimethylthiazoline (TMT) while we simultaneously recorded metabolic rates. We observed no increase in metabolic rate in mice that were exposed to TMT, compared with mice that were exposed to a control odour (Extended Data Fig. 6h,i). These data suggest that the increase in metabolic rate on T1 was due not to a general stress response but specifically to the recall of a cold memory.

Finally, to demonstrate the behavioural expression of a cold memory, we analysed whether mice develop a conditioned cold aversion due to training at 4 °C in a conditioned place preference apparatus (Extended Data Fig. 6j). Mice have no preference for either side of the apparatus on the day before the test at 21 °C (Extended Data Fig. 6k); however, mice trained at 4 °C displayed a conditioned place aversion to the cold-paired side of the conditioned place preference apparatus but not to the 21 °C paired side (Extended Data Fig. 6l). These data demonstrate that mice can form a contextual memory of a cold environment that, after retrieval, leads to an increase in whole-body metabolism and avoidance behaviour.

Cold memories upregulate thermogenesis

BAT is a specialized tissue that is important for non-shivering thermogenesis in both humans and rodents[24]. The lipolysis metabolic pathway has been demonstrated to fuel the thermogenic response in brown adipocytes through uncoupling protein 1 (UCP-1)[25] (Fig. 1m). To further establish the relationship between cold memory and whole-body metabolic responses, we collected BAT from mice at different time points (Fig. 1m). In line with previous studies, we showed that after cold exposure, multiple thermogenic genes are upregulated, including *Ucp1* (Extended Data Fig. 7b–g). Notably, we found that several thermogenic genes are also upregulated in mice during cold recall on T1, compared with control mice on BL2 (Fig. 1n–s). We observed an upregulation of *Ucp1* (Fig. 1n), in addition to an increase in mitochondrial genes involved in fatty acid uptake, such as *Cpt1a* (which encodes CPT1α) and *Cact* (Fig. 1o,p) and genes associated with fatty acid release from lipid droplets, such as *Atgl* and *Hsl* (Fig. 1q,r). These results indicate that recall of a cold memory is sufficient to upregulate thermogenic genes in BAT.

We tested whether the observed upregulation of thermogenesis genes was specifically due to cold experiences or due to a generalized stress response. We collected BAT from mice that underwent contextual fear conditioning training and compared them with mice that received no foot shocks (Extended Data Fig. 7h). We observed no differences in any of the examined thermogenesis genes between mice that received foot shocks and controls that did not (Extended Data Fig. 7i–n).

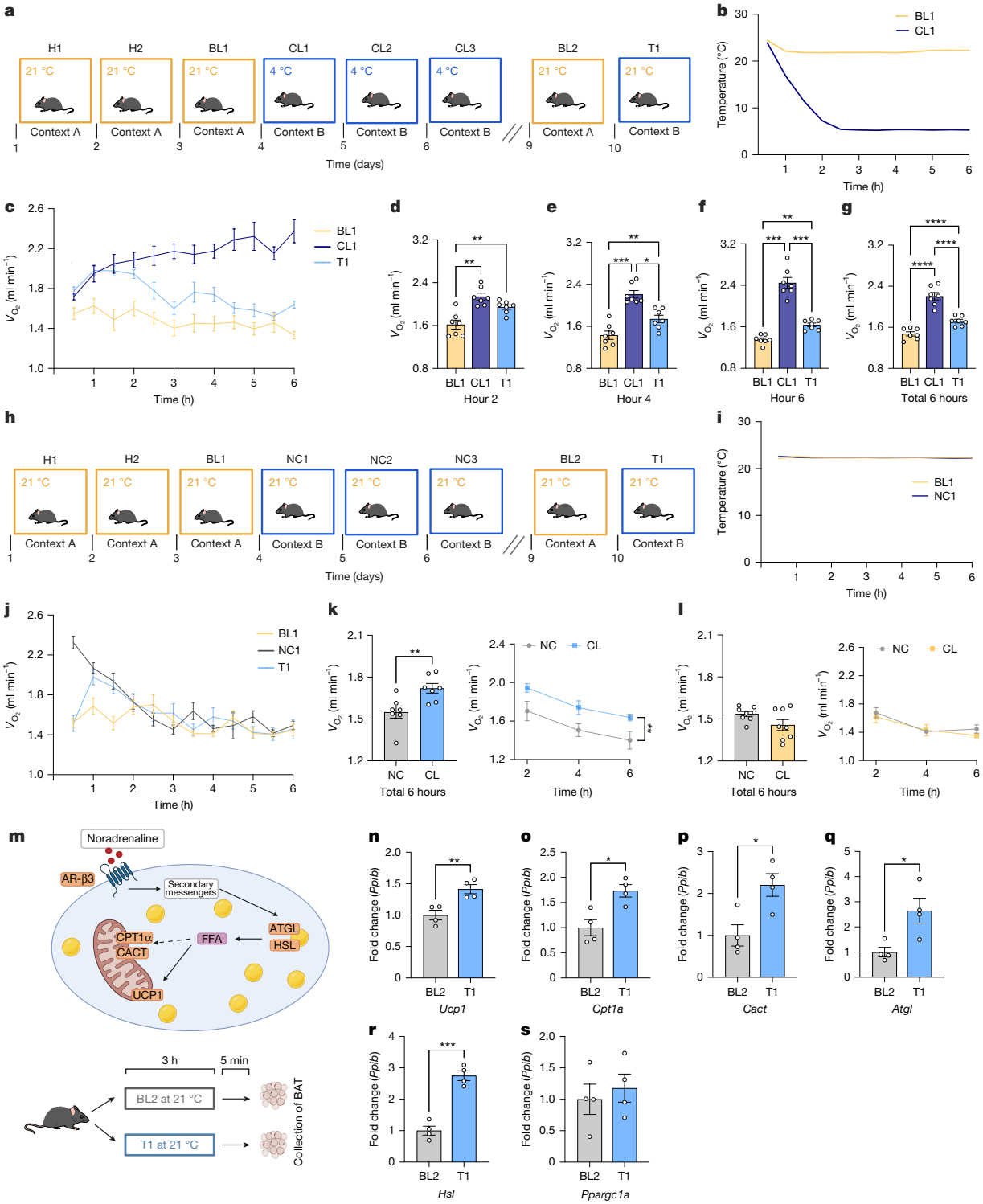

Fig. 1 | Contextual cold memories increase metabolic rate and thermogenic gene expression. a, Experimental timeline. **b**, Environmental temperature during baseline 1 (BL1, yellow) and cold day 1 (CL1, dark blue). **c**, Time plot of oxygen consumption between mice during BL1 (yellow), T1 (test, light blue) and CL1 (dark blue). **d**–**g**, Comparison of oxygen consumption between mice during BL1 (yellow), T1 (light blue) and CL1 (dark blue) at hour 2 (**d**), hour 4 (**e**) and hour 6 (**f**) and for the total time averaged in metabolic cages (**g**). **h**, Experimental control timeline. **i**, Environmental temperature during BL1 (yellow) and NC1 (no cold 1, dark blue). **j**, Time plot of oxygen consumption between mice during BL1 (yellow), T1 (light blue) and NC1 (dark blue). **k**, Comparison of oxygen consumption between the cold-paired (light blue) and no-cold-paired (grey) cohorts on the test day (6 h averaged; left) and at hours 2, 4 and 6 (right). **l**, Comparison of oxygen consumption between the cold-paired (yellow) and no-cold-paired (grey) cohorts on BL1 (6 h averaged; left) and at hours 2, 4 and 6 (right). **m**, Thermogenic pathway in BAT and experimental timeline. **n**–**s**, Relative expression of lipolysis and thermogenesis genes (*Ucp1* (**n**), *Cpt1a* (**o**), *Cact* (**p**), *Atgl* (**q**), *Hsl* (**r**) and *Ppargc1a* (which encodes PGC1α; **s**)) in the BAT of mice during BL2 (grey) compared with T1 (blue). **c**–**g**,**j**–**l**,**n**–**s**, Data are mean ± s.e.m., $n = 4$–8 mice per group. **d**–**g**, Repeated measures analysis of variance (ANOVA). **k**–**l**, Unpaired *t*-test and two-way repeated measures ANOVA. **n**–**s**, Unpaired *t*-test. $^{*}P < 0.05$, $^{**}P < 0.01$, $^{***}P < 0.001$, $^{****}P < 0.0001$. CL2, cold day 2; CL3, cold day 3; FFA, free fatty acid; H1, habituation day 1; H2, habituation day 2; NC2, no cold 2; NC3, no cold 3; V_{O_2}, oxygen consumption. Illustrations of timeline (**a**), adipocyte lipolysis (**m**, top) and tissue collection (**m**, bottom) were created in BioRender (https://biorender.com).

Next, we collected BAT from mice that were exposed to a predator odour (TMT) or to a neutral control odour (H_2O, Extended Data Fig. 7o). We found no increase in thermogenic gene expression in mice exposed to TMT compared with mice that were exposed to H_2O (Extended Data Fig. 7p–u). However, we found significantly decreased expression of *Hsl* in TMT-exposed mice compared with H_2O-exposed controls (Extended Data Fig. 7t). Together, these experiments showed that thermogenesis genes in BAT are not upregulated as a result of a stressful experience in general, but that this increase is due to a cold experience specifically. We therefore conclude that cold memories can control whole-body thermoregulatory responses.

Cold memories enhance activity in specific brain regions

To identify the neuronal activity patterns that underlie cold memory encoding and retrieval, we examined FOS expression throughout multiple brain regions. We compared FOS activity during BL1, CL1 and T1, to determine which regions were active during specific conditions (Fig. 2a). To enable automated FOS detection in various hippocampal and hypothalamic regions, all brains were run through an automated brain-wide counting pipeline (Fig. 2b,c). Our results showed no differences in the number of FOS^+ cells in the dentate gyrus (DG) between any of the three examined conditions (Fig. 2d). However, cold-activated FOS activity was found in the CA3 and CA1 subregions of the hippocampus at CL1 and T1, compared with BL1, suggesting that CA3 and CA1 are important areas that are involved in cold responses (Fig. 2e,f). Although no innate differences in FOS activity were found in the DG between the three conditions, we hypothesized that there may be differences in how this region interacts with whole-body metabolism after learning. As such, we correlated FOS activity in the DG with oxygen consumption at BL1, CL1 and T1 (Fig. 2g). Our results showed that at BL1, there was no correlation between FOS activity in the DG and metabolic rate. At CL1, there was a negative correlation between oxygen consumption and DG activity. However, at T1, after the cold memory has been consolidated, there was a significant positive correlation between oxygen consumption and DG activity (Fig. 2g). A similar correlation pattern was observed in CA1 but not in CA3 (Extended Data Fig. 8a,b). We conclude that various subregions of the hippocampus are involved in the encoding or retrieval of contextual cold memories and that the DG and CA1 play a part in regulating whole-body metabolism at T1.

Previous studies have identified the LHA, MPO and lateral preoptic area (LPO) as key brain regions involved in thermoregulation[26]. We therefore compared FOS activity in these regions at BL1, CL1 and T1. In line with previous studies, we showed that FOS activity in the LHA is upregulated when mice are exposed to the cold during CL1 (Fig. 2h). Notably, we found similar levels of activity in this area when mice are recalling the cold on T1. Although we also see increased activity in the MPO and LPO during cold exposure (Fig. 2i,j), we found no increases in FOS activity in these areas on T1. Moreover, no increases in FOS activity were found at CL1 or T1 in any of the other investigated hypothalamic areas (Extended Data Fig. 8h–k). Next, we tested whether activity in the LHA, MPO and LPO correlated with metabolic rate. We found that only the mice that were exposed to the cold on CL1 show a positive correlative trend between FOS activity in the LHA and oxygen consumption (Fig. 2k). This trend was not found in any other condition or hypothalamic region (Extended Data Fig. 8c,d). These findings suggest that the LHA is important during encoding and recall of cold and that LHA activity correlates with metabolic rate during a cold experience.

Finally, to confirm that the increases in FOS activity found during CL1 and T1 were specifically due to cold exposure and recall rather than because of stress, mice were trained in a fear conditioning experiment (Extended Data Fig. 9a). Mice that underwent contextual fear conditioning training did not show similar increases in FOS activity in hippocampal or hypothalamic regions to those observed in the cold (Extended Data Fig. 9c–j). Furthermore, increased FOS activity was observed in amygdalar regions after fear conditioning, but not during the cold or cold recall (Extended Data Figs. 8m–o and 9l–n). These data suggest that stress was not the cause of the neural activity found in the hippocampus and hypothalamus.

To understand how functional connectivity between brain regions is altered during cold exposure and cold-memory retrieval, we performed further correlational analyses of FOS activity across brain regions (Extended Data Fig. 8r–t). From this, we built correlational networks that corresponded to BL1, CL1 and T1 to further visualize plasticity of functional connectivity (Fig. 2l–n). We found that, compared with the baseline network, there is increased functional connectivity between hypothalamic regions when mice are exposed to the cold (Fig. 2l,m). Moreover, we found an increase in functional connectivity between the hippocampus and the hypothalamus when mice are recalling the cold, compared with when they are experiencing the cold, which is not observed in the baseline network (Fig. 2l–n). These data suggest that hippocampus-to-hypothalamus connectivity is a plasticity feature that forms after a cold contextual memory is encoded in mice.

Cold engrams are in the DG, LHA and MPO

Engram ensembles have been identified in many areas of the brain, such as the hippocampus, amygdala and prefrontal cortex, for various sensory modalities[19,27–32]. To better understand how cold memories are encoded and retrieved, we crossed *Trap2* mice with *R26R*-STOP-floxed enhanced yellow fluorescent protein (*eYFP*) transgenic mice to achieve optimal labelling in the DG, LHA, MPO and LPO[19,33,34] (Fig. 3a).

To quantify activated engram cells in multiple brain regions, mice were put through a cold-engram-labelling protocol (Fig. 3b). The number of $eYFP^+$ cells was first quantified in the DG, LHA, MPO and LPO (Fig. 3c). Our findings show no differences in the number of $eYFP^+$ cells in the DG, LHA, MPO or LPO between mice recalling a contextual cold memory at T1 and home-cage controls, suggesting comparable amounts of labelled cells in both groups (Fig. 3d–g). Next, we quantified the number of FOS^+ cells between the groups (Fig. 3h–l). There was a significant increase in the number of FOS^+ cells in mice retrieving the cold memory in the LHA (Fig. 3j), whereas no significant differences were found in the DG, MPO and LPO (Fig. 3i,k,l). Finally, we measured engram reactivation by quantifying the cells that were active during both encoding and expression of a cold memory (that is, $(FOS^+eYFP^+)/eYFP^+$; Fig. 3m). Our results show a significant increase in colabelling in the DG, LHA and MPO (Fig. 3n,o,p), but not in the LPO (Fig. 3q), in mice retrieving a cold memory compared with home-cage controls. Together, these data suggest that cold-sensitive memory engrams are located in the DG, LHA and MPO.

We next analysed how increased reactivation of cold-sensitive engrams affected whole-body metabolism. Here we correlated the amount of colabelled cells in the DG with oxygen consumption, carbon dioxide production and energy expenditure. We found strong positive correlations between cold-engram cell reactivation in the DG and metabolic rate at T1 and CL1, but not at BL1 (Fig. 3r–t). These results indicate that increased cold engram reactivation during recall covaries with whole-body metabolism during recall, and, crucially, with metabolism during the original training day when the engram was formed. Finally, we performed correlational analyses of engram reactivation activity across brain regions. These analyses revealed a significant positive correlation between activity in the DG and LHA in mice recalling the cold (Fig. 3u), whereas this type of coordinated activity was not found in the home-cage control mice (Fig. 3v). Similarly, we found coordinated activity between the MPO and LPO in test mice but not in controls (Fig. 3u–v). In line with our FOS data, these results indicate that when mice recall the cold, a specific engram pathway emerges between the DG and LHA, in addition to a connection between the MPO and LPO, and that coordinated hypothalamic activity is essential for contextual cold memories.

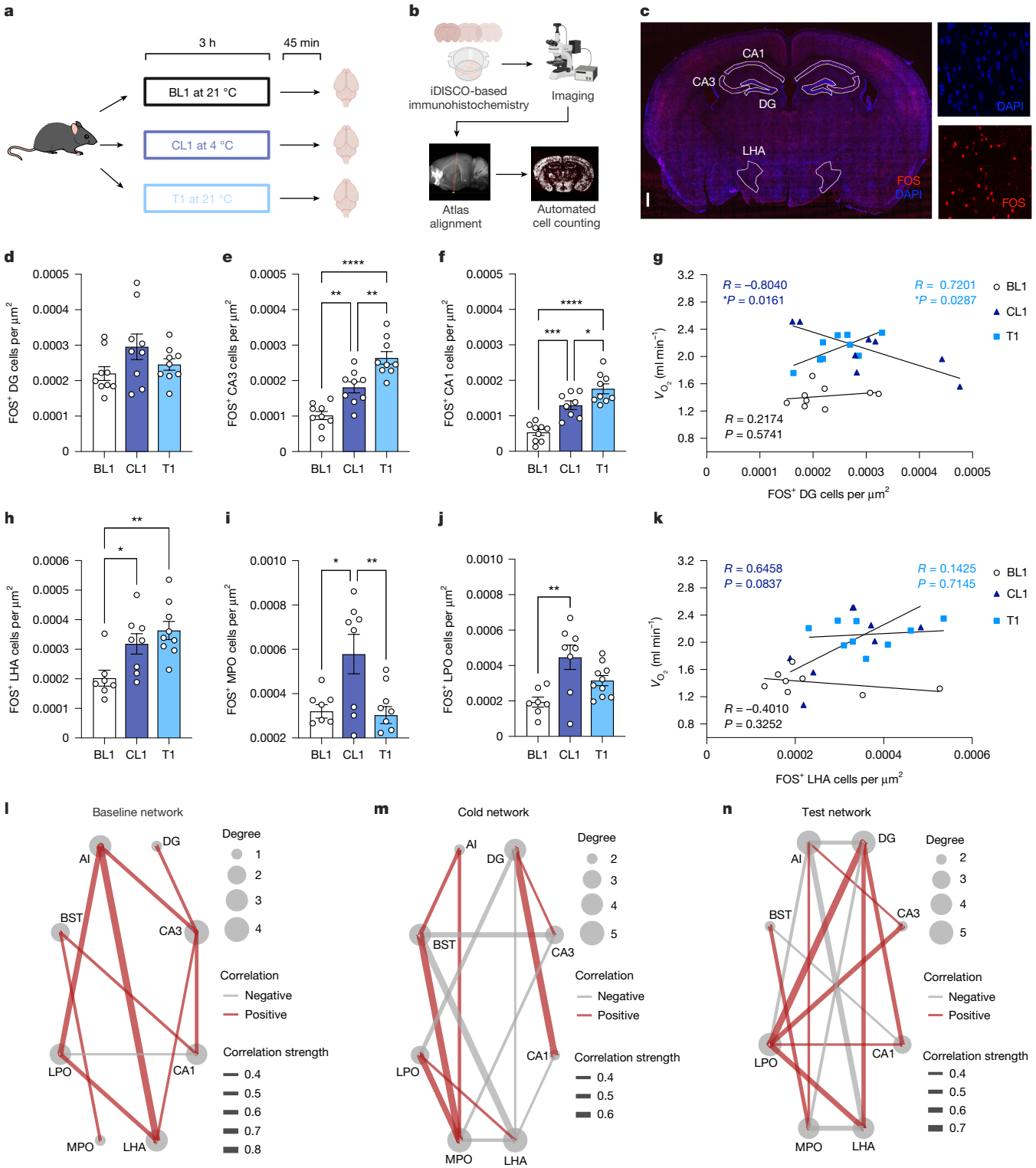

Fig. 2 | Contextual cold memories are encoded and retrieved in the hippocampus and hypothalamus. a, Experimental timeline for tissue collection. **b**, Automated brain-wide FOS detection pipeline used to identify FOS$^+$ cells in multiple brain regions simultaneously. iDISCO, immunolabelling-enabled imaging of solvent-cleared organs. **c**, Hippocampal slice (left) with FOS$^+$ cells (red; bottom right) and DAPI$^+$ cells (blue; top right). Scale bar, 500 µm. **d**–**f**, Comparison of FOS$^+$ neurons normalized to area in the DG (**d**), CA3 (**e**) and CA1 (**f**) between mice during BL1 (white), CL1 (dark blue) and T1 (light blue). **g**, Correlation between FOS$^+$ cells in the DG and oxygen consumption between mice during BL1 (white), CL1 (dark blue) and T1 (light blue). **h**–**j**, Comparison of FOS$^+$ neurons normalized to area in the LHA (**h**), MPO (**i**) and LPO (**j**) between mice during BL1 (white), CL1 (dark blue) and T1 (light blue). **k**, Correlation between FOS$^+$ cells in the LHA and oxygen consumption between mice during BL1 (white), CL1 (dark blue) and T1 (light blue). **l**–**n**, Correlation analysis of FOS$^+$ cells between brain regions at BL1 (**l**), CL1 (**m**) and T1 (**n**). Correlations with $R > 0.5$ are displayed in red. Correlations with $R < 0.5$ are displayed in grey. Line thickness is proportional to the strength of the correlation (R value). **d**–**f**,**h**–**j**, Data are mean ± s.e.m., **d**–**n**, $n = 7$–10 mice per group. **d**–**f**,**h**–**j**, One-way ANOVA. **g**,**k**, Simple linear regression with slope comparison. $^*P < 0.05$, $^{**}P < 0.01$, $^{***}P < 0.001$, $^{****}P < 0.0001$. Illustration of the tissue collection **a** and schematic in **b** created with BioRender (https://biorender.com).

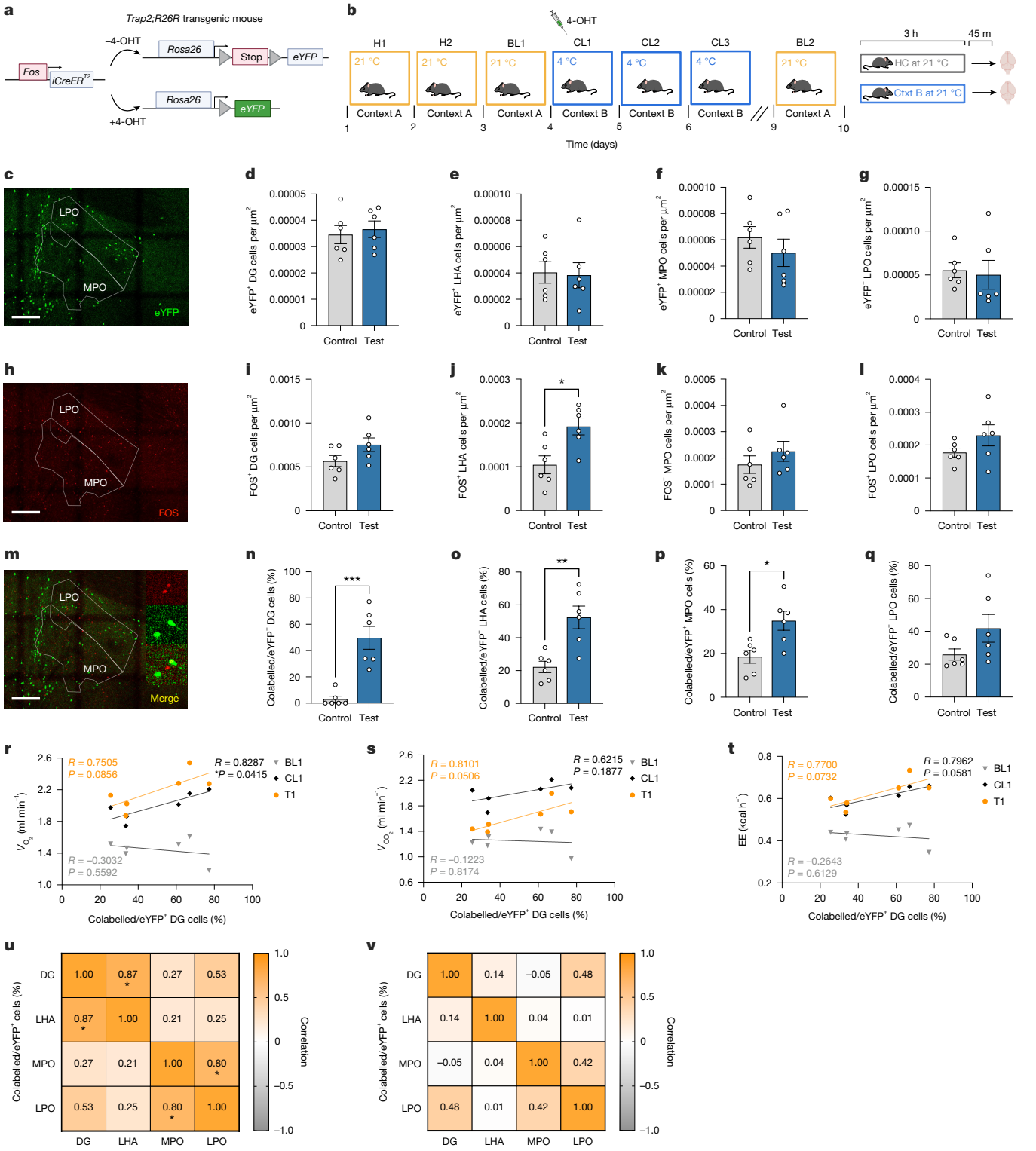

Fig. 3 | Putative contextual cold engrams are in the DG, LHA and MPO. **a**, Genetic strategy. **b**, Experimental timeline. **c**, Representative image of eYFP$^+$ cells (green). **d**–**g**, Comparison between the test cohort (dark blue) and control cohort of eYFP$^+$ neurons normalized to area (grey) in the DG (**d**), the LHA (**e**), the MPO (**f**) and the LPO (**g**). **h**, Representative image of FOS$^+$ cells (red). **i**–**l**, Comparison between the test cohort (dark blue) and control cohort (grey) of FOS$^+$ neurons normalized to area in the DG (**i**), the LHA (**j**), the MPO (**k**) and the LPO (**l**). **m**, Representative image of an eYFP$^+$FOS$^+$ cell. **n**–**q**, Comparison between the test cohort (dark blue) and control cohort (grey) of colabelled neurons in the DG (**n**), the LHA (**o**), the MPO (**p**) and the LPO (**q**). **r**–**t**, Correlation between the percentage of colabelled/eYFP$^+$ cells in the DG and oxygen consumption (**r**) carbon dioxide production (**s**) and energy expenditure (EE, **t**) at T1 (orange), CL1 (black) and BL1 (grey). **u**, Correlation of percentage of colabelled/eYFP$^+$ cells between regions during the recall of a cold memory on T1. **v**, Correlation of percentage of colabelled/eYFP$^+$ cells in the control group. **c**–**q**, Data are mean ± s.e.m., $n = 6$ mice per group. **d**–**g**,**i**–**l**,**n**–**q**, Unpaired *t*-test. **r**–**t**, Simple linear regression. **u**,**v**, Pearson's *r* correlation analysis. $^*P < 0.05$, $^{**}P < 0.01$, $^{***}P < 0.001$. 4-OHT, 4-hydroxytamoxifen; $\dot{V}_{CO_2}$, carbon dioxide production; Ctxt, context; HC, home cage. Scale bars, 250 µm. Illustrations of the transgenic mouse line (**a**) and the behavioural time line (**b**) were created with BioRender (https://biorender.com).

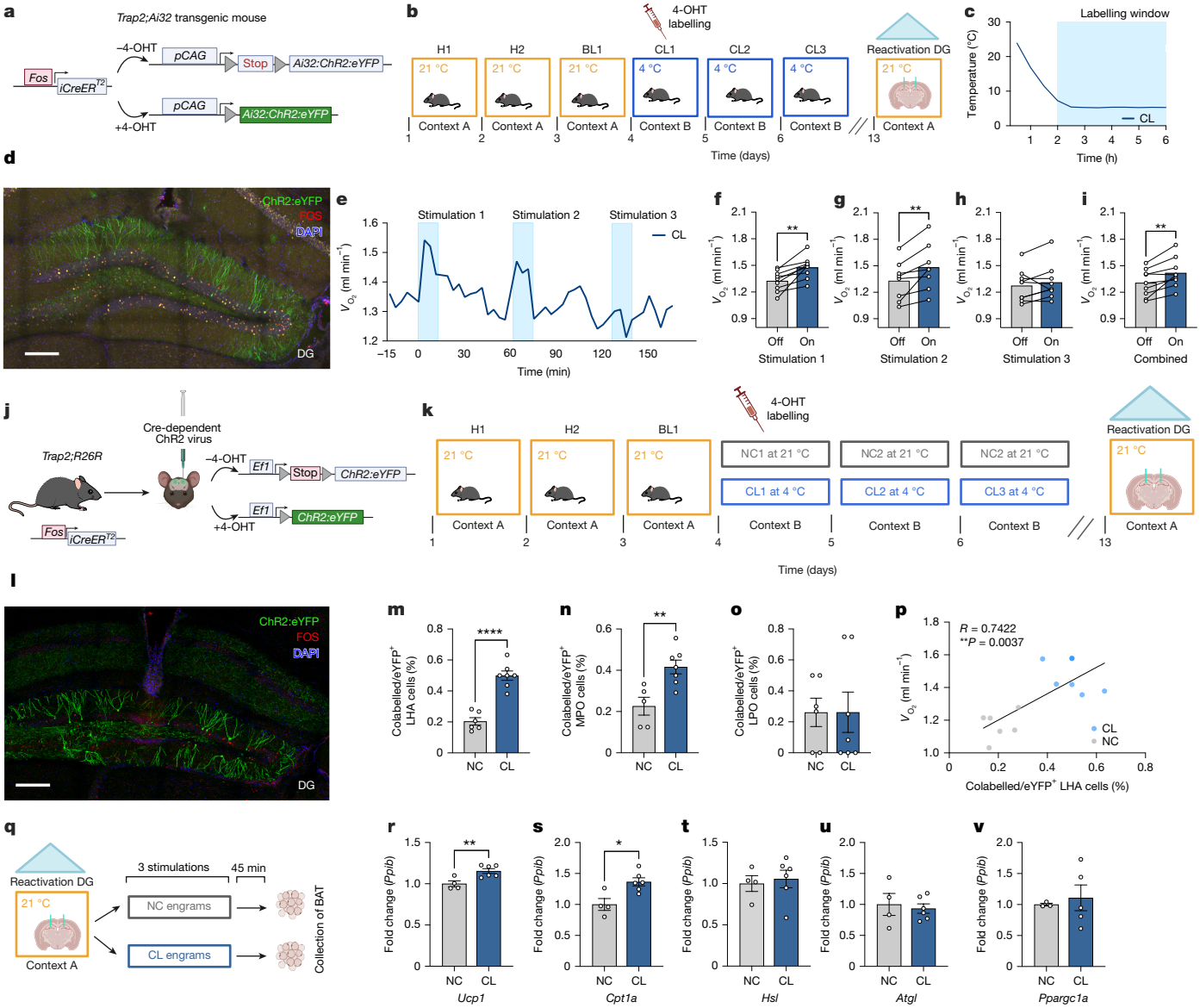

Fig. 4 | Artificial reactivation of cold-sensitive engrams in the DG increases metabolism and thermogenesis genes. a, Genetic strategy. **b**, Experimental timeline. **c**, Environmental temperature during the labelling window. **d**, Representative image of hippocampal slice with FOS$^+$ cells (red) and eYFP$^+$ cells (green). **e**, Time plot of oxygen consumption during artificial reactivation of cold-sensitive engrams. Blue bars indicate the time the laser was turned on. **f**–**h**, Comparison of oxygen consumption between the on (blue) and off (grey) epochs during the three stimulations. **i**, Comparison of oxygen consumption between the on (blue) and off (grey) epochs of cold-sensitive cells during all stimulations combined. **j**, Genetic strategy. **k**, Experimental timeline. **l**, Representative image of a hippocampal slice with FOS$^+$ cells (red) and eYFP$^+$ cells (green). **m**–**o**, Comparison of colabelled neurons between the cold-stimulated cohort (dark blue) and the no-cold-stimulated control cohort (grey) in the LHA (**m**), the MPO (**n**) and the LPO (**o**). **p**, Correlation between the percentage of colabelled/eYFP$^+$ cells in the LHA and oxygen consumption after cold stimulation (blue) and no-cold stimulation (grey). **q**, Experimental timeline. **r**–**v**, Relative expression of lipolysis and thermogenesis genes (*Ucp1* (**r**), *Cpt1a* (**s**), *Hsl* (**t**), *Atgl* (**u**) and *Ppargc1a* (**v**)) in the BAT of mice with cold-sensitive stimulated cells (blue) and no-cold control-stimulated cells (grey). **e**–**i**, Data are mean, $n = 8$–9 mice per group. **m**–**p**,**r**–**v**, Data are mean ± s.e.m., $n = 5$–7 mice per group. **e**–**i**, Paired *t*-test. **m**–**o**, Unpaired *t*-test. **p**, Simple linear regression. **r**–**v**, Unpaired *t*-test. $^*P < 0.05$, $^{**}P < 0.01$, $^{***}P < 0.001$, $^{****}P < 0.0001$. ChR2, channelrhodopsin. Scale bars (**d**, **l**), 250 µm. Illustrations of the transgenic labelling systems (**a**,**j**), the behavioural timelines (**b**,**k**) and the tissue collection timeline (**q**) were created with BioRender (https://biorender.com).

Cold engram stimulation increases metabolism

To determine whether cold-sensitive engrams are functionally relevant for whole-body metabolism, we set out to optogenetically reactivate cold engrams in the DG. To do so, we labelled cold-sensitive engrams in the DG on CL1 and optogenetically reactivated them in a neutral context (Fig. 4a–d and Extended Data Fig. 10a–c). We showed that optogenetic reactivation of cold-sensitive engrams in the DG is sufficient to artificially increase whole-body metabolism (Fig. 4e and Extended Data Fig. 11j,l). Moreover, we found that metabolic rates increased when cold-sensitive engrams were stimulated, and that they returned to baseline during the unstimulated period (Fig. 4f–i). Notably, metabolic rate increased only in the first two consecutive stimulations, but not during a third stimulation, suggesting an attenuation of whole-body responses or a limitation of optogenetic engram stimulation (Fig. 4h). Furthermore, we demonstrated that optogenetic reactivation of cold-sensitive engrams is possible with multiple transgenic mouse lines and with different engram-labelling strategies, including one based on the FOS-tTa system (Extended Data Fig. 12a–h).

To confirm that the increase in metabolic rate was due to contextual cold memories, we designed a control experiment in which mice were run through the same timeline but were never exposed to the cold (Extended Data Fig. 11a,b). As such, we labelled no-cold engram cells in the DG and optogenetically reactivated them in a neutral context. Our results show that optogenetically stimulating no-cold engram cells does not increase whole-body metabolism (Extended Data Fig. 11c,k,m). There were no significant differences between on and off periods during any of the three stimulations (Extended Data Fig. 11d–g). Notably, a slight decrease in oxygen consumption was found when the laser was on compared with when it was off (Extended Data Fig. 11g). We next directly compared optogenetic stimulation of cold-sensitive engrams with no-cold contextual engrams (Extended Data Fig. 11h). We show that oxygen consumption significantly increased in the cold group compared with the no-cold group during laser stimulation (Extended Data Fig. 11i). The difference in metabolic rate during laser activation was not due to pre-existing differences between the cohorts, as no differences were found between the cold and no-cold groups when the laser was off (Extended Data Fig. 11i). Therefore, we conclude that cold-sensitive engrams control whole-body metabolism, as optogenetic activation of these cells increases metabolic rate.

We investigated whether optogenetic stimulation of cold-sensitive DG engrams would result in increased engram activity in hypothalamic regions. To achieve this, we labelled cold engrams in the DG with channelrhodopsin on CL1, while labelling engrams throughout the brain with eYFP on a background of the *Trap2;R26R* compound transgenic line. We subsequently quantified artificially reactivated engram cells in the LHA, MPO and LPO (Fig. 4j–l). We show that there was a significant increase in colabelling (that is, (FOS^+eYFP^+)/$eYFP^+$) in the LHA and MPO after optogenetic stimulation of cold-sensitive DG engrams compared with after stimulation of no-cold engrams (Fig. 4m–o and Extended Data Fig. 12i–r). This increase in colabelling was not found in the LPO (Fig. 4o), suggesting that only specific regions of the hypothalamus have increased engram connectivity with the DG. Notably, we found that the artificially induced engram activity in the LHA significantly correlated with oxygen consumption (Fig. 4p), suggesting that the connectivity found between the DG and specific regions of the hypothalamus mediates the learned control of whole-body metabolism.

Next, we optogenetically reactivated cold-sensitive engrams to artificially induce a thermogenic response and collected BAT to determine whether artificial reactivation of cold memories increases thermogenic gene expression in adipose tissue (Fig. 4q). Our results show that artificial reactivation of a cold-sensitive engram leads to an increase in *Ucp1* (Fig. 4r) and *Cpt1a* (Fig. 4s) expression in BAT compared with the reactivation of no-cold engram cells. No differences were found in other thermogenic genes (Fig. 4t–v). Together, these results show that both natural and artificial retrieval of cold memories causes an upregulation of thermogenesis genes in BAT.

Inhibiting cold engrams blocks metabolic change

To further explore the role of cold-sensitive engram cells, we chemogenetically inhibited DG cold engrams during cold-memory recall. To do so, we labelled cold-sensitive engrams in the DG of the hippocampus on CL1 with inhibitory DREADD (designer receptors exclusively activated by designer drugs) hM4Di receptors and chemogenetically inhibited these cells by injecting clozapine-*N*-oxide (CNO)[35] on T1 (Fig. 5a–c and Extended Data Fig. 10d–g). We observed an increase in metabolic rate on T1 compared with BL1 when saline was injected into control mice on T1. This increase in metabolic rate was observed throughout the 2 h and for the combined total testing time (Fig. 5d–g and Extended Data Fig. 13b,c,g,h). By contrast, we found that CNO-treated mice no longer showed the learned increase in metabolic rate on T1 (Fig. 5h). Furthermore, we found that the conditioned response was no longer present at any point throughout the testing time (Fig. 5h–k and Extended Data Fig. 13d,e,i,j). When directly comparing the saline- and CNO-injected mice, we found a significantly higher percentage change in metabolism in the saline-injected mice than in the CNO-injected mice (Fig. 5l–n and Extended Data Fig. 13f,k). Together, these data show that by inhibiting cold-sensitive cells in the DG, we could inhibit contextual cold memories and, as a result, prevent the conditioned whole-body responses that were previously associated with these contextual stimuli.

Discussion

In this study, we investigated the influence of memory engrams on whole-body responses. We found that mice increase their metabolic rate, core body temperature and adjust their behaviour when recalling a cold environment, indicating that they can store and recall temperature information. Our findings reveal that the recall of a cold environment increases FOS activity in the hippocampus and hypothalamus and that it leads to increased functional connectivity between these two structures. We found that cold-sensitive engram cells are located in the DG, LHA and MPO and that artificial reactivation of DG engram cells leads to an increase in whole-body metabolism and engram cell activity in the hypothalamus. Moreover, our results showed that inhibition of cold-sensitive cells in the DG prevents the conditioned whole-body response that was previously associated with cold memories. Notably, we show that contextual cold memories control whole-body responses in BAT by increasing thermogenic genes during cold recall. Together, these data show that cold-sensitive engrams control whole-body thermoregulatory responses.

Previous studies have demonstrated a direct role for the hypothalamus in regulating body temperature, heart rate and energy expenditure[36–40]. In this study, we link memories to changes in whole-body metabolism. The increases found here are not solely due to a general stress response to the cold, as we found that exposure to other stressful experiences did not increase metabolic rate or expression of lipolytic and thermogenic genes. Although cold exposure may inevitably cause some stress to the mice, it does not explain the memory outcomes found here. However, it was not possible to completely exclude the possibility of cold being a mild pain or discomfort signal in this study. We found no differences in food consumption during cold exposure or cold memory recall, suggesting that 8 h of cold exposure is not long enough to cause changes in feeding behaviour, which is in line with previously reported results[4]. Notably, we found that mice increased their movement across training days and when recalling the cold, indicating that previous experience and expectations causes adaptive behavioural responses in mice.

Previous studies investigating the role of the hippocampus after acute heat and cold exposure showed a distinct role of the DG only after acute heat exposure[41]. In line with this, we found no differences in FOS activity in the DG after cold exposure. However, we found significant increases in neuronal activity in CA3 and CA1, suggesting that both of these areas potentially hold innate cold-sensing cells. Future experiments are needed to determine whether these hippocampal subregions are important for innate cold responses. By comparing the cells that were active during the encoding and recall of a cold memory, we found putative cold-sensitive memory engrams in the DG, LHA and MPO. Previous studies have shown that engram cells are necessary and sufficient to induce the learning-specific conditioned behavioural response, and that neural activity can regulate immune responses[10,17,30]. Here we describe how engram cells control peripheral physiological processes beyond traditionally studied behavioural responses. Our results show that contextual cold engrams in the DG control whole-body metabolism through engram connectivity in the LHA and MPO. Furthermore, we show that engram connectivity in the hypothalamus resulting from artificial DG stimulation correlates with whole-body metabolism. One question that remains is whether these bodily responses in turn also influence engram cells specifically and

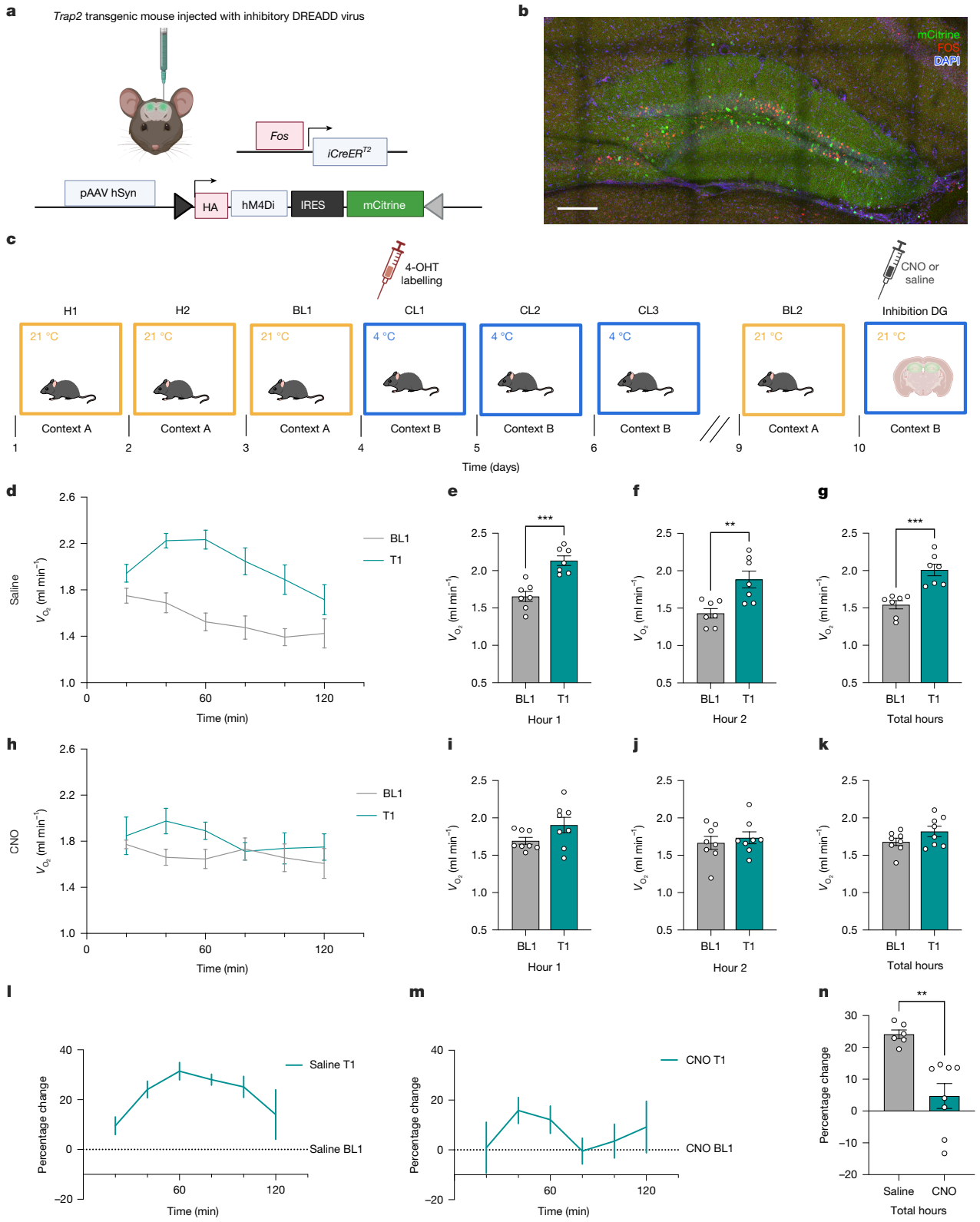

Fig. 5 | Inhibition of cold-sensitive engrams prevents the memory effects on oxygen consumption. **a**, Genetic strategy. **b**, Representative image of a hippocampal slice with FOS$^+$ cells (red) and mCitrine$^+$ cells (green). Scale bar, 250 µm. **c**, Experimental timeline. **d**, Time plot of oxygen consumption of saline-injected mice during BL1 (grey) and T1 (teal). **e**–**g**, Comparison of oxygen consumption of saline-injected mice during BL1 (grey) and T1 (teal) at hour one, hour two and total time averaged. **h**, Time plot of oxygen consumption of CNO-injected mice during BL1 (grey) and T1 (teal). **i**–**k**, Comparison of oxygen consumption of CNO-injected mice during BL1 (grey) and T1 (teal) at hour one, hour two and total time averaged. **l**, Time plot of the percentage change in oxygen consumption on T1 (teal) compared with BL1 (black) in saline-injected mice. **m**, Time plot of the percentage change in oxygen consumption on T1 (teal) compared with BL1 (black) in CNO-injected mice. **n**, Comparison of the percentage change in oxygen consumption between saline-injected (grey) and CNO-injected (teal) mice on T1. Data are mean ± s.e.m., **d**–**n**, $n = 7$–8 mice per group. **e**–**g**,**i**–**k**, Paired t-test. **n**, Unpaired t-test. $^{**}P < 0.01$, $^{***}P < 0.001$. Illustration of the transgenic labelling system (**a**) and the behavioural timeline (**c**) were created with BioRender (https://biorender.com).

memories in general. For example, increasing heart rate by optogenetic activation of cardiac rhythms resulted in enhanced anxiety[42]. It is therefore highly likely that information flows not only from the brain to the body but also vice versa. Future studies are necessary to determine how bodily states modulate the storage and formation of memories and how this relates to engram cells.

BAT has been found to be a versatile organ that is involved in a variety of metabolic and endocrine processes. Recently, it has also been suggested that BAT might be a stress-responsive organ that is crucial for a fight-or-flight response[43,44]. Here we show that the genes in the thermogenic pathway analysed in this study are not uniquely activated by stress. Moreover, our results revealed no differences in thermogenic gene expression in fear-conditioned or predator-odour-exposed mice. As such, we found that these genes are specifically involved in thermoregulatory processes that are activated when a mouse is encoding and recalling a cold environment. Together, our data and previously published data seem to suggest that different types of stressor elicit different responses from BAT and that its response is highly dependent on the type of contextual input that it receives.

Our findings may have important translational implications for potential treatment avenues for metabolic diseases. In humans, BAT has been associated with cardiometabolic health, making it a promising target for future therapies[45–47]. In this study, we aimed to understand how the brain affects basic bodily functions with the additional goal of identifying therapeutic targets that would enable more-targeted treatments for cardiometabolic diseases in the future. For example, we showed that by stimulating engram cells in the brain, we were able to upregulate thermogenesis genes in BAT. With the current technological advancements of optogenetics in humans, this line of research opens interesting avenues for future therapeutic approaches.

Online content

Any methods, additional references, Nature Portfolio reporting summaries, source data, extended data, supplementary information, acknowledgements, peer review information; details of author contributions and competing interests; and statements of data and code availability are available at https://doi.org/10.1038/s41586-025-08902-6.

1. Tan, C. L. & Knight, Z. A. Regulation of body temperature by the nervous system. *Neuron* **98**, 31–48 (2018).
2. Morrison, S. F. & Nakamura, K. Central mechanisms for thermoregulation. *Annu. Rev. Physiol.* **81**, 285–308 (2019).
3. Jung, S. et al. A forebrain neural substrate for behavioral thermoregulation. *Neuron* **110**, 266–279 (2022).
4. Lal, N. K. et al. Xiphoid nucleus of the midline thalamus controls cold-induced food seeking. *Nature* **621**, 138–145 (2023).
5. Finger, S. *Minds Behind the Brain: A History of the Pioneers and Their Discoveries* (Oxford Univ. Press, 2004).
6. Ben-Shaanan, T. L. et al. Modulation of anti-tumor immunity by the brain's reward system. *Nat. Commun.* **9**, 2723 (2018).
7. Chan, K. L., Poller, W. C., Swirski, F. K. & Russo, S. J. Central regulation of stress-evoked peripheral immune responses. *Nat. Rev. Neurosci.* **24**, 591–604 (2023).
8. Cryan, J. F. et al. The microbiota–gut–brain axis. *Physiol. Rev.* **99**, 1877–2013 (2019).
9. Haykin, H. et al. Reward system activation improves recovery from acute myocardial infarction. *Nat. Cardiovasc. Res.* **3**, 841–856 (2024).
10. Koren, T. et al. Insular cortex neurons encode and retrieve specific immune responses. *Cell* **184**, 5902–5915 (2021).
11. Morrison, S. F., Madden, C. J. & Tupone, D. Central neural regulation of brown adipose tissue thermogenesis and energy expenditure. *Cell Metab.* **19**, 741–756 (2014).
12. Morrison, S. F., Madden, C. J. & Tupone, D. Central control of brown adipose tissue thermogenesis. *Front. Endocrinol.* **3**, 5 (2012).
13. Nakamura, K. & Morrison, S. F. A thermosensory pathway that controls body temperature. *Nat. Neurosci.* **11**, 62–71 (2008).
14. Semon, R. W. & Semon, R. W. *Die Mneme als erhaltendes Prinzip im Wechsel des organischen Geschehens* (Engelmann, 1920).
15. Denny, C. A., Lebois, E. & Ramirez, S. From engrams to pathologies of the brain. *Front. Neural Circuits* **11**, 23 (2017).
16. Josselyn, S. A. & Tonegawa, S. Memory engrams: recalling the past and imagining the future. *Science* **367**, eaaw4325 (2020).
17. Liu, X. et al. Optogenetic stimulation of a hippocampal engram activates fear memory recall. *Nature* **484**, 381–385 (2012).
18. Ryan, T. J., Ortega-de San Luis, C., Pezzoli, M. & Sen, S. Engram cell connectivity: an evolving substrate for information storage. *Curr. Opin. Neurobiol.* **67**, 215–225 (2021).
19. Denny, C. A. et al. Hippocampal memory traces are differentially modulated by experience, time, and adult neurogenesis. *Neuron* **83**, 189–201 (2014).
20. Reijmers, L. G., Perkins, B. L., Matsuo, N. & Mayford, M. Localization of a stable neural correlate of associative memory. *Science* **317**, 1230–1233 (2007).
21. Cannon, B. & Nedergaard, J. Brown adipose tissue: function and physiological significance. *Physiol. Rev.* **84**, 277–359 (2004).
22. Cohen, P. & Kajimura, S. The cellular and functional complexity of thermogenic fat. *Nat. Rev. Mol. Cell Biol.* **22**, 393–409 (2021).
23. Fischer, A. W., Cannon, B. & Nedergaard, J. Optimal housing temperatures for mice to mimic the thermal environment of humans: an experimental study. *Mol. Metab.* **7**, 161–170 (2018).
24. Betz, M. J. & Enerbäck, S. Human brown adipose tissue: what we have learned so far. *Diabetes* **64**, 2352–2360 (2015).
25. Bargut, T. C. L., Aguila, M. B. & Mandarim-de-Lacerda, C. A. Brown adipose tissue: updates in cellular and molecular biology. *Tissue Cell* **48**, 452–460 (2016).
26. Morrison, S. F. & Nakamura, K. Central neural pathways for thermoregulation. *Front. Biosci.* **16**, 74–104 (2011).
27. Ramirez, S. et al. Creating a false memory in the hippocampus. *Science* **341**, 387–391 (2013).
28. Redondo, R. L. et al. Bidirectional switch of the valence associated with a hippocampal contextual memory engram. *Nature* **513**, 426–430 (2014).
29. Cowansage, K. K. et al. Direct reactivation of a coherent neocortical memory of context. *Neuron* **84**, 432–441 (2014).
30. Ryan, T. J., Roy, D. S., Pignatelli, M., Arons, A. & Tonegawa, S. Engram cells retain memory under retrograde amnesia. *Science* **348**, 1007–1013 (2015).
31. Tonegawa, S., Liu, X., Ramirez, S. & Redondo, R. Memory engram cells have come of age. *Neuron* **87**, 918–931 (2015).
32. Santos, S. L. et al. Propranolol decreases fear expression by modulating fear memory traces. *Biol. Psychiatry* **89**, 1150–1161 (2021).
33. DeNardo, L. A. et al. Temporal evolution of cortical ensembles promoting remote memory retrieval. *Nat. Neurosci.* **22**, 460–469 (2019).
34. Srinivas, S. et al. Cre reporter strains produced by targeted insertion of *EYFP* and *ECFP* into the *ROSA26* locus. *BMC Dev. Biol.* **1**, 4 (2001).
35. Roth, B. L. DREADDs for neuroscientists. *Neuron* **89**, 683–694 (2016).
36. Contreras, C., Nogueiras, R., Diéguez, C., Rahmouni, K. & López, M. Traveling from the hypothalamus to the adipose tissue: the thermogenic pathway. *Redox Biol.* **12**, 854–863 (2017).
37. Piñol, R. A. et al. *Brs3* neurons in the mouse dorsomedial hypothalamus regulate body temperature, energy expenditure, and heart rate, but not food intake. *Nat. Neurosci.* **21**, 1530–1540 (2018).
38. Piñol, R. A. et al. Preoptic BRS3 neurons increase body temperature and heart rate via multiple pathways. *Cell Metab.* **33**, 1389–1403 (2021).
39. Stefanidis, A., Wiedmann, N. M., Adler, E. S. & Oldfield, B. J. Hypothalamic control of adipose tissue. *Best Pract. Res. Clin. Endocrinol. Metab.* **28**, 685–701 (2014).
40. Tan, C. L. et al. Warm-sensitive neurons that control body temperature. *Cell* **167**, 47–59 (2016).
41. Bachtell, R. K., Tsivkovskaia, N. O. & Ryabinin, A. E. Identification of temperature-sensitive neural circuits in mice using c-Fos expression mapping. *Brain Res.* **960**, 157–164 (2003).
42. Hsueh, B. et al. Cardiogenic control of affective behavioural state. *Nature* **615**, 292–299 (2023).
43. Kataoka, N., Hioki, H., Kaneko, T. & Nakamura, K. Psychological stress activates a dorsomedial hypothalamus–medullary raphe circuit driving brown adipose tissue thermogenesis and hyperthermia. *Cell Metab.* **20**, 346–358 (2014).
44. Qing, H. et al. Origin and function of stress-induced IL-6 in murine models. *Cell* **182**, 372–387 (2020).
45. Cypess, A. M. et al. Activation of human brown adipose tissue by a β3-adrenergic receptor agonist. *Cell Metab.* **21**, 33–38 (2015).
46. Becher, T. et al. Brown adipose tissue is associated with cardiometabolic health. *Nat. Med.* **27**, 58–65 (2021).
47. Stanford, K. I. et al. Brown adipose tissue regulates glucose homeostasis and insulin sensitivity. *J. Clin. Invest.* **123**, 215–223 (2013).

Methods

Mice

All experiments with wild-type mice were performed with C57BL/6J mice. All engram-labelling experiments were performed with *Fos-tTa*[17,20], *Trap2;Ai32* (refs. 33,48) and *Trap2;R26R* (refs. 19,34) transgenic mice. Both male and female mice were used. All mice were group housed in a 12:12-h (07:00–19:00) light–dark colony room at 22 °C. Food and water were provided ad libitum and all testing was performed during the light phase. Mice used for experiments were approximately 8–12 weeks of age. All animal work was performed in compliance with the Ryan and Lynch laboratory project licences, with ethical approval of the Trinity College Dublin ethics committee, the Animal Research Ethics Committee from the Health Products Regulatory Authority, and according to the Brigham and Women's Hospital Institutional Animal Care and Use Committee guidelines.

Metabolic cages

To capture metabolic and behavioural information, mice were singly housed in metabolic cages (Promethion, Sable Systems) for a duration of 8 h per day. Each cage included a ceiling-mounted food hopper, water bottle and body-mass monitor. Mice had ad libitum access to food and water throughout the entire 8 h. Oxygen consumption, carbon dioxide emission, energy expenditure, body weight, food and water intake and locomotor activity were monitored throughout the session. In brief, respiratory gasses were measured with an integrated fuel cell oxygen analyser, a spectrophotometric carbon dioxide analyser and a water vapour pressure analyser (GA3m1, Sable Systems)[49]. Before each run, gas sensors were calibrated with 100% N_2 as zero reference and with a span gas containing a known concentration of 0.933% CO_2. Air flow was measured and controlled with the multichannel mass flow generator (FR8-1, Sable Systems). Flow rate was set at 2,000 ml min^{-1}. Oxygen consumption and carbon dioxide production were measured for each mouse at 3–4-min intervals. Energy expenditure was calculated using the equation[50]: $K_{cal/h} = 60 \times (0.0003941 \times V_{O_2} + 0.001106 \times V_{CO_2}$.

Cold training schedule

Male mice were taken from their home cage each morning and individually housed in the Promethion cages for a maximum of 8 h. On days 1 and 2, mice were placed in the Promethion cages at 21 °C to allow them to habituate to the machine. On day 3, mice were put in the Promethion cages at 21 °C while metabolic and behavioural data were simultaneously recorded to establish baseline measurements (context A). On day 4, the cages were changed before the mice were placed inside. Contextual cues were added to the chambers, including wall and floor patterns, brighter lights, different bedding and three drops of acetic acid odour (context B). Once the mice were placed in the cages, the temperature decreased in increments of approximately 10 °C per hour. As such, the mice spent a total of 6 h in the altered context at a temperature of 4 °C. This was repeated for a total of three days, with metabolic and behavioural data recorded throughout. Mice were then returned and kept in their home cages for a two-day break period. Next, on day 9, mice were put back in the Promethion cages without any of the additional cues at 21 °C to allow for a second baseline measurement (context A). Finally, on day 10 all the additional context cues were added back in before the mice were put into the cages (context B). Temperature was kept at 21 °C and metabolic and behavioural data were simultaneously recorded to establish the test-day measurements.

Predator odour exposure in metabolic cages

Mice were placed in the metabolic cages 24 h before odour application. In brief, 20 µl of either H_2O or 10% w/v trimethylthiazoline were dropped onto a small 1-cm square piece of filter paper in the cage. Mice were exposed to the odorant for 1 h before being put back into their home cage. Metabolic data were recorded at all times.

Conditioned cold aversion

The conditioned place preference apparatus consisted of two separate chambers. Each chamber had different wall and floor cues (black and white pattern). Mice could freely enter both chambers through an opening in the wall in the middle of the apparatus. On day 1, mice were taken from their home cage and placed inside the apparatus, where they could freely explore both sides of the apparatus for a total of 20 min. The entire apparatus was kept at 21 °C. On day 2, the opening in the middle wall of the apparatus was closed. During the morning sessions, mice were exposed to one side of the apparatus at 21 °C for a duration of 2 h. Mice were then returned to their home cage for a 2-h break. In the afternoon sessions, mice were then exposed to the other side of the apparatus at 4 °C for a duration of 2 h. This was subsequently repeated for a total of three days. On day 5, the opening in the middle wall of the apparatus was re-opened before mice were placed back in the apparatus. Mice could freely explore both chambers again for a total of 20 min while the entire apparatus was kept at 21 °C. All behaviours were videotaped and subsequently hand scored. Time spent in each chamber in seconds was measured on day 1 (pre-test) and day 5 (test). The time spent in each chamber was normalized using the formula (test phase duration spent in the cold-paired chamber/time spent there in the pre-test phase), to account for any pre-existing preferences[51]. Both time of day and side of apparatus were counterbalanced across all mice.

Contextual fear conditioning

Before training, mice were handled for three consecutive days to habituate them to the experimenter. One day before the training day, mice were habituated to the arena and allowed to freely explore the context for 10 min. The next day, mice underwent a contextual fear conditioning protocol. The mice were allowed to explore the arena for the first 3 min. After these 3 min, half of the mice received three foot shocks (0.2 s, 0.75 mA) that were spaced by intervals of 1 min, whereas the other half of the mice received no foot shocks. Mice were subsequently returned to their home cage for 45 min.

Predator odour exposure for BAT collection

Mice were placed into a vacuum-powered four-chamber olfactory arena, which was replicated from previously published designs[52]. Air entered each corner of the arena at a flow rate of 150 ml min^{-1} and was odorized by passing through a bottle containing 20 ml of H_2O or 350 mM trimethylthiazoline. Mice were exposed to the odour for 5 min and were then euthanized for tissue collection.

Tissue collection

Cold memory. Brains and BAT were collected from mice that went through the above-described cold memory timeline. Tissues were collected on BL1, CL1, BL2 and T1. To ensure that the differences seen were due to the differences in conditions and not time of day, all tissues were collected exactly 5 h after the mice were put inside the Promethion cages.

Contextual fear conditioning. For the contextual fear conditioning experiments, brains and BAT were collected 45 min after the training session ended.

Predator odour exposure. For the predator odour exposure experiments, BAT was collected exactly 1 h after the mice were exposed to the odours.

Tissue preparation

Brains. Mice were transcardially perfused with 4% paraformaldehyde and brains were fixed in 4% paraformaldehyde overnight. The next day, brains were transferred into phosphate-buffered saline (PBS) and kept

at 4 °C. They were subsequently sliced in 100-µm coronal sections with a vibratome (Leica VT1200 S) and collected in PBS.

BAT. Mice were euthanized by carbon dioxide inhalation and adipose tissue was removed by making a careful incision between the shoulder blades. Interscapular BAT was subsequently collected, snap frozen in liquid nitrogen and stored at −80 °C.

Immunohistochemistry

To get clear immunolabelling, we used the previously described iDISCO-based immunohistochemistry protocol[53,54]. Sections were rinsed three times in 1× PBS before being dehydrated in 50% MeOH/PBS at room temperature for 2.5 h. Sections were then rinsed three times in 0.2% PBS with Triton X-100 and blocked in 0.2% PBS with Triton X-100 containing 10% dimethyl sulfoxide and 6% normal goat serum for 2 h at room temperature. After blocking, slides were washed three times in PBS with 0.2% Tween-20 and 10 µg ml^{-1} heparin (PTwH). Sections were then incubated with primary antibodies (chicken polyclonal anti-GFP (1:1,000, Invitrogen) and rabbit polyclonal IgG anti-FOS (1:1,000, Synaptic Systems)) at 4 °C on a shaker for three days in PTwH with 5% dimethyl sulfoxide and 3% normal goat serum. On day 4, sections were washed three times in PTwH and incubated with secondary antibodies (Alexa Fluor 568 anti-rabbit IgG (1:500, Invitrogen) and Alexa Fluor 488 anti-chicken IgG (1:500, Invitrogen)) overnight at 4 °C. The next day, sections were washed three times in PTwH, followed by three washes in PBS at room temperature. Finally, sections were stained with DAPI in PBS for 10 min followed by a final wash in PBS. Sections were then mounted on superfrost slides using Vectashield DAPI, cover-slipped and sealed.

Confocal imaging

All images were taken on a confocal scanning microscope (Leica TCS SP8, Leica Microsystems). Fluorescence from DAPI was detected at 417–488 nm, Alexa Fluor 568 was detected at 595–650 nm and Alexa Fluor 488 was detected at 500–550 nm. Sections were imaged with a dry 20× objective (NA 0.70, working distance 0.5 mm), with a pixel size of 1.14 × 1.14 µm^2, a *z* step of 3 µm and a *z* stack of approximately 25 µm. Fields of view were stitched together to form tiled images using an automated stage and the algorithm of the LAS X software.

Automated cell counting

To perform automatic brain-wide analysis of FOS$^+$ cells, we used the NeuroInfo software (MBF Bioscience). In brief, immunohistochemistry-labelled whole-brain sections were aligned to the Allen Mouse Brain Atlas using the registration tool in the program[55]. Here brain sections were matched to the most closely corresponding atlas plate. All sections were manually adjusted where necessary, to ensure accurate fit. After the correct atlas plate was identified, all anatomical regions of interest were delineated and measured for size in µm^2. Next, FOS$^+$ cells were identified using the cell-detection workflow. Throughout all sections, only cells between 7 µm and 19 µm were counted for size consistency. These parameters were then combined with a deep-learning algorithm to successfully identify FOS$^+$ cells. Counts were then checked for accuracy and adjusted where necessary. Finally, detected cells were mapped to the Allen Mouse Brain Atlas and tallied in the corresponding anatomical brain structure. Normalized counts (cells per µm) were subsequently plotted into GraphPad Prism 10.0 for further analysis.

Network analysis

Cross-correlations between all pairs of regions were calculated in R as previously reported[32]. Pearson's correlations were computed in all cases after which networks were created using the igraph package. To be able to interpret the networks, correlations with an absolute value below 0.5 were not included. Both positive and negative correlations were included in the networks.

Metabolic rate and cell activity analysis

To investigate whether FOS and engram activity correlated with metabolic rate, we correlated FOS$^+$ and colabelled eYFP$^+$ (%) with the exact metabolic rate (oxygen consumption, carbon dioxide production and energy expenditure) that was measured 45 min before brain collection.

RNA extraction and qPCR analysis

Collected BAT was defrosted at room temperature and transferred to a 2-ml tube, and stainless-steel beads were added to each individual tube. Next, tissues were homogenized in 1 ml TRIzol reagent in a tissue lyser for 2.5 min at 25 pulses per second. Chloroform (200 µl) was subsequently added to each tube, after which they were inverted and left at room temperature for 3 min. All tubes were then centrifuged at 12,000*g* for 15 min, the RNA was transferred into a new tube and 500 µl isopropanol was added to precipitate the RNA. All tubes were inverted ten times and left at room temperature for 10 min, before being centrifuged again at 12,000*g* for 10 min. Supernatants were then discarded and all remaining RNA pellets were washed in 1 ml of 25% RNase-free dH_2O and 75% ethanol. After being centrifuged at 12,000*g* for 5 min, all supernatants were discarded by inverting the tube. RNA pellets were left to dry at room temperature for 20–30 min until they were transparent, after which they were resuspended in 50 µl RNase-free water. Finally, RNA was left on ice for 30 min and subsequently put on a heat block at 55 °C for 15 min. A Nanodrop 2000 UV spectrophotometer (Thermo Fisher Scientific) was used to assess RNA quality and concentration. Next, 20 µl cDNA was synthesized from 2 µg of isolated RNA using a cDNA reverse transcription kit (Biosciences Ltd) in a MiniAmp Thermal Cycler (BD Biosciences). qPCRs were then performed to quantify the relative mRNA expression of genes of interest. Relative mRNA levels were calculated using the ΔΔ cycle threshold ($\Delta\Delta C_t$) method and normalized to corresponding endogenous controls (*Ppib*). All calculated values were plotted into GraphPad Prism 10 for further analysis.

Stereotactic surgeries

Optic fibre implants. Mice that were used in the optogenetic experiments were implanted with a custom implant containing two optic fibres (200 mm core diameter; Doric Lenses). The optic fibre implant was lowered above the injection site at −1.75 mm dorsoventral. To secure the implant, an even layer of Metabond (C&B Metabond) was applied and left to dry for 15 min. A protective cap was then made from a black polypropylene microcentrifuge tube and secured with dental cement. Animals were then put in a recovery chamber at 29 °C until they were fully recovered from the anaesthesia before being returned to their home cage. Animals were allowed to recover from surgery for approximately 2–3 weeks before behavioural testing.

Viral injections. FOS-tTa transgenic mice were put on a diet containing doxycycline (DOX) 48 h before surgeries. All surgeries were performed when the mice were approximately 7–8 weeks old. Mice were anaesthetized with 500 mg kg^{-1} avertin and head-fixed on a stereotaxic frame. Bilateral craniotomies were performed using a 0.5-mm diameter drill at −2.00 mm anteroposterior and ±1.35 mm mediolateral. Next, 300 µl AAV9-TRE-ChR2-eYFP was injected on each side using a microsyringe pump (UMP3; WPI) and a Hamilton syringe (701LT; Hamilton) at −2.00 mm anteroposterior, ±1.35 mm mediolateral and −2.00 mm dorsoventral. The injection speed was 60 nl min^{-1} and the needle was left inside for an additional 10 min after virus delivery to achieve maximum virus spread.

For chemogenetic experiments, TRAP2 mice were injected with 300 µl pAAV-hSyn-DIO-HA-hM4D(Gi)-IRES-mCitrine on each side at −2.00 mm anteroposterior, ±1.35 mm mediolateral and −2.00 mm dorsoventral. The injection speed was 60 nl min^{-1}.

Temperature probe surgery

Before implantation, all temperature probes were sterilized. Mice were anaesthetized and positioned on their back as previously described[56]. Next, all of the skin around the stomach area was sanitized with 70% ethanol and sterilized saline. A small incision was made using a scalpel in the middle of the abdomen, followed by a 1-cm incision in the peritoneum. A temperature probe was subsequently put in the abdominal cavity. Organs were placed over the probe before sewing the peritoneum and skin with sterile stitches.

Labelling strategies

TRAP2 strategy. The TRAP2 system enables the permanent labelling of neurons that were activated by a given experience[57]. TRAP2 relies on an immediate early gene locus to drive the expression of iCre recombinase combined with a transgenic Cre-dependent effector. The iCre recombinase can be controlled by tamoxifen. As such, when a neuron is active and tamoxifen or 4-OHT is present, the iCre recombinase can enter the nucleus and result in expression of the effector[33]. The TRAP2 mice were combined with two different reporter lines. For optogenetic experiments, TRAP2 mice were bred with the *Ai32* mice[48]. For engram cell-counting experiments, TRAP2 mice were crossed with the *R26R* mice[34].

To label the cells that were activated during a cold experience, mice were injected with tamoxifen 5 h after being put in the Promethion cages on CL1. As such, all cells that were active during the 6-h cold exposure were labelled. All mice were returned to their home cages immediately after labelling.

FOS-tTa strategy. Here we used an adeno-associated virus that expresses channelrhodopsin-2 (ChR2)–eYFP under the control of a tetracycline-responsive element (TRE)-containing promoter (AAV9-TRE-ChR2-eYFP). The TRE promoter is only active in cells that contain the tetracycline transactivator (tTa)[42]. Therefore, we injected the AAV9-TRE-ChR2-eYFP virus into the DG of *Fos-tTa* transgenic mice. These mice express tTa under the control of a *Fos* promoter[20]. Because FOS is activity dependent, the *Fos-tTa* transgene will only express tTa in cells that are active during a given experience. By combining the transgenic mice with the virus, we were able to express tTa and ChR2–eYFP in cells that were active during a cold experience. To have temporal control over this system, mice were put on a diet that contained DOX. DOX is an antibiotic that binds to tTa and as such prevents the expression of the transgene *ChR2-eYFP*.

To label cells activated by a cold experience, DOX food was substituted with standard food 36 h before being exposed to a cold experience. Cold memory engrams were identified as the cells that expressed ChR2–eYFP as a result of being active during the cold. To close the labelling window, mice were immediately put back on DOX food after the initial cold experience.

4-OHT

To label cold-sensitive engrams in *Trap2;Ai32* and *Trap2;R26R* transgenic mice, we intraperitoneally injected mice with 4-OHT (50 mg kg^{-1}, Santa Cruz). All 4-OHT was freshly prepared on the labelling day in a mix of sunflower seed oil and castor oil (4:1, Sigma-Aldrich) at 10 mg ml^{-1}.

Engram tagging

To identify the cells that were active during a cold experience, we used *Trap2;R26R* mice. These mice were chosen because they showed more reliable labelling in the hypothalamus than did other mice. In brief, all mice were injected with tamoxifen 5 h after being put in the Promethion cages on CL1 to label all cells that were active during the 6-h cold exposure. Next, mice were exposed to the rest of the cold memory timeline as described above (two additional training days, a 2-day break and BL2). On the test day, half of the mice were put into context B at 21 °C and half of the mice were kept in their home cage. After exactly 3 h and 45 min all mice were euthanized to enable visualization of the immediate early gene *Fos*.

Engram counting

All cells were counted using Fiji[58]. An investigator blinded to treatment counted $eYFP^+$, FOS^+ and colabelled cells bilaterally in the DG, LHA, MPO and the LPO. All cell counts were normalized to their respective areas and plotted as cells per μm^2.

Optogenetic reactivation of cold memories in metabolic cages

Shining 472-nm blue light on a ChR2-expressing cell causes ChR2 channels to open, resulting in the depolarization of the neuron. This enables us to evoke memory recall in mice with ChR2-labelled cells. Optogenetic activation was performed through a 450-nm laser diode fibre light source (Doric LDFLS 450/080). Mice with optic fibre implants were attached to a patch cord (MFP_200/240/900-0.22_0.3m_FC-ZF1.25(F)) and allowed to habituate for 8 h before being put through the above-described cold memory timeline. Cold-sensitive engrams were labelled on CL1 and optogenetic reactivation was performed one week later in context A. On the reactivation day, mice were exposed to a 15-min optogenetic stimulation (8 mA) session that was divided into 3-min on and 1-min off periods (that is, 3 min on, followed by 1 min off). During the light-on period, mice received blue-light stimulation (20 Hz) with a pulse width of 15 ms for the entire 3-min duration. During the light-off period, the mice received no light stimulation. To enable animals to return to baseline, each 15-min stimulation period was followed by 1 h of no light stimulation. Mice received a total of three rounds of 15-min stimulation periods. Metabolic rates were measured at all times.

Chemogenetic inhibition of cold memories in metabolic cages

To inhibit cold engrams, we used the same labelling timeline as described above. In brief, mice went through two habituation days and a baseline measurement day in context A, at 21 °C. On day 4, contextual cues were added to the chambers and the mice spent a total of 6 h in the altered context at a temperature of 4 °C. To label the neurons that were active during these 6 h of 4 °C cold exposure, mice were injected with 4-OHT 5 h after being put in the Promethion cages. All mice were returned to their home cages immediately after labelling. Mice subsequently went through two additional training days and were then kept in their home cages for a two-day break period. On day 9, mice were put back in the Promethion cages without any of the additional cues at 21 °C to allow for a second baseline measurement (context A). Finally, on day 10, half of the mice were injected with CNO (2 mg kg^{-1}, Tocris) and half of the mice were injected with saline. Mice were kept in their home cage for 30 min after injection and were then put in the Promethion cages (context B, 21 °C).

Statistics

All data were analysed using GraphPad Prism 10. All data are mean ± s.e.m. An α level of 0.05 was used as a criterion for statistical significance and probability levels were quoted for non-significance. All statistical analyses performed are reported with their outcomes in Supplementary Data 1 and 2.

Figure design and visualization

Illustrations were created with BioRender (www.biorender.com).

Inclusion and diversity

We support inclusive, diverse and equitable conduct of research.

Reporting summary

Further information on research design is available in the Nature Portfolio Reporting Summary linked to this article.

Data availability

In this study the Allen Brain Atlas was used as a reference for brain regions. This database is publicly available at https://mouse.brain-map.org/static/atlas. All data necessary for the interpretation and replication of the reported findings are contained in the Article and Supplemental Information. Statistical and detailed figure source data are provided in the Supplemental Information. Raw data supporting the findings of this study are available from the corresponding author upon reasonable request.

48. Madisen, L. et al. A toolbox of Cre-dependent optogenetic transgenic mice for light-induced activation and silencing. *Nat. Neurosci.* **15**, 793–802 (2012).
49. Kothari, V. et al. High fat diet induces brain insulin resistance and cognitive impairment in mice. *Biochim. Biophys. Acta* **1863**, 499–508 (2017).
50. de V. Weir, J. B. New methods for calculating metabolic rate with special reference to protein metabolism. *J. Physiol.* **109**, 1–9 (1949).
51. Golden, S. A. et al. Basal forebrain projections to the lateral habenula modulate aggression reward. *Nature* **534**, 688–692 (2016).
52. Root, C. M., Denny, C. A., Hen, R. & Axel, R. The participation of cortical amygdala in innate, odour-driven behaviour. *Nature* **515**, 269–273 (2014).
53. Renier, N. et al. iDISCO: a simple, rapid method to immunolabel large tissue samples for volume imaging. *Cell* **159**, 896–910 (2014).
54. Pavlova, I. P., Shipley, S. C., Lanio, M., Hen, R. & Denny, C. A. Optimization of immunolabeling and clearing techniques for indelibly labeled memory traces. *Hippocampus* **28**, 523–535 (2018).
55. Tappan, S. J. et al. Automatic navigation system for the mouse brain. *J. Comp. Neurol.* **527**, 2200–2211 (2019).
56. Takahashi, T. M., Sakurai, T. & Hirano, A. Measuring body temperature of freely moving mice under an optogenetics-induced long-term hypothermic state. *STAR Protoc.* **4**, 102321 (2023).
57. Guenthner, C. J., Miyamichi, K., Yang, H. H., Heller, H. C. & Luo, L. Permanent genetic access to transiently active neurons via TRAP: targeted recombination in active populations. *Neuron* **78**, 773–784 (2013).
58. Schindelin, J. et al. Fiji: an open-source platform for biological-image analysis. *Nat. Methods* **9**, 676–682 (2012).

Acknowledgements We thank T. Boto and past and present members of the Ryan laboratory for scientific discussions and support, B. Schramm, G. McManus and R. Rakhmatullin for their continuous technical support and E. Stewart for proofreading. This work was funded by the US Air Force Office of Scientific Research (FA9550-24-1-0258 and FA9550-20-1-0316), European Research Council (715968), Irish Research Council (GOIPG/2020/913), Science Foundation Ireland (15/YI/3187), the National Institute of Health (1R01NS121316), the Canadian Institute for Advanced Research, and core support from Trinity College Dublin.

Author contributions Conceptualization and scientific design: A.M.Z., A.D. and T.J.R. Methodology: A.M.Z., A.D., P.B.C., C.A.D., L.L. and T.J.R. Investigation: A.M.Z., A.D., P.B.C., E.U., T.M., L.M., C.O.S. and J.D.O. Data interpretation: A.M.Z, A.D., P.B.C., C.A.D., C.O.S., L.L. and T.J.R. Funding acquisition: T.J.R. Project administration: A.M.Z. and T.J.R. Supervision: T.J.R. Writing of the original draft: A.M.Z and T.J.R. All authors contributed to writing and editing.

Competing interests C.A.D. is named on provisional and non-provisional patent applications for the prophylactic use of (*R*,*S*)-ketamine and related compounds against stress-induced psychiatric disorders. A.M.Z., A.D., P.B.C., T.M., E.U., J.D.O.L., L.M., C.O.S., L.L. and T.J.R. declare no competing interests.

Additional information

Supplementary information The online version contains supplementary material available at https://doi.org/10.1038/s41586-025-08902-6.

Correspondence and requests for materials should be addressed to Tomás J. Ryan.

Peer review information *Nature* thanks Marc Reitman, Abha Rajbhandari and the other, anonymous, reviewer(s) for their contribution to the peer review of this work. Peer reviewer reports are available.

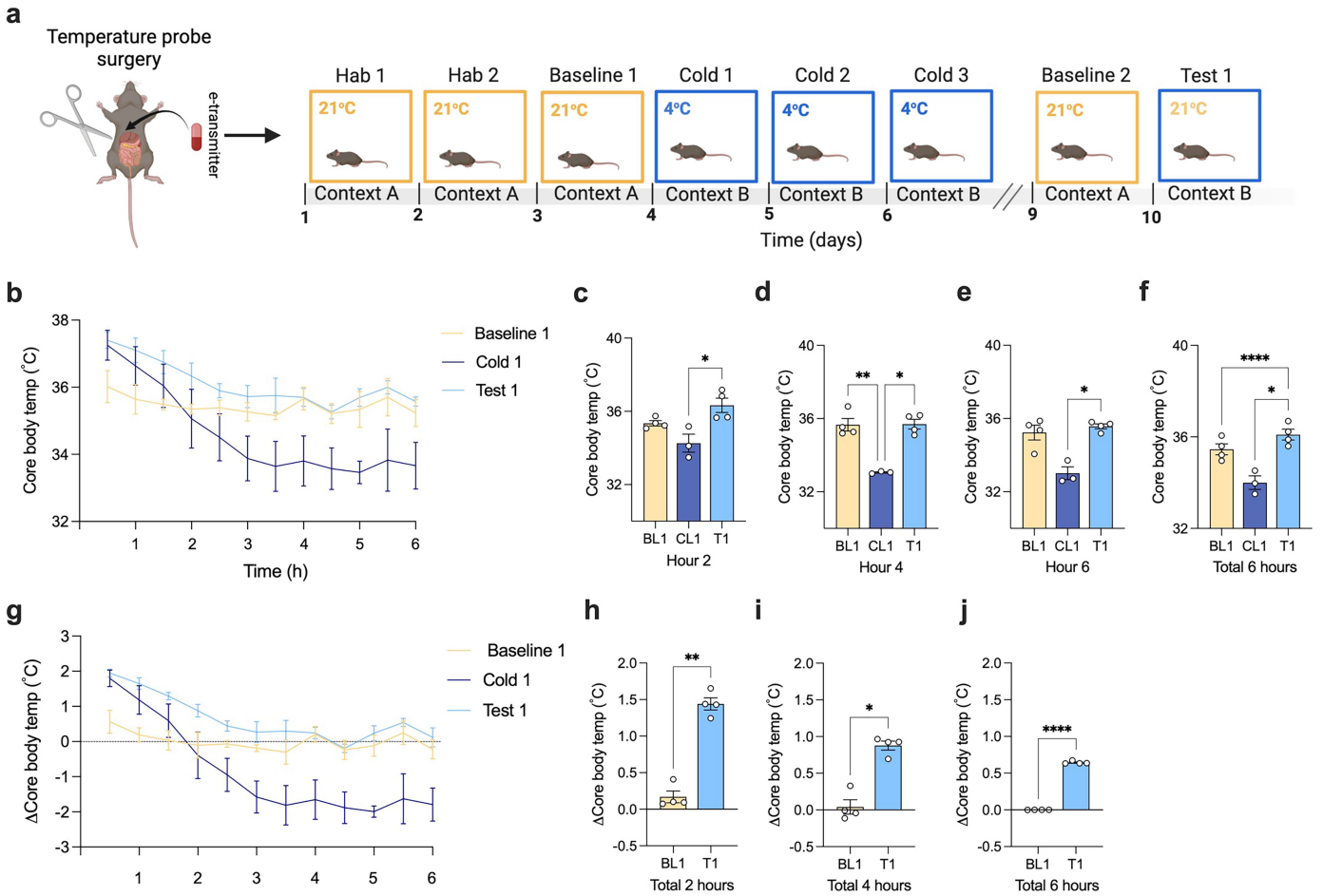

Extended Data Fig. 1 | Retrieval of a contextual cold memory increases core body temperature. a Diagrammatic representation of experimental timeline. **b** Time plot of core body temperature between mice during Baseline 1 (21 °C; yellow), Test 1 (21 °C; light blue) and Cold 1 (4 °C; dark blue). Comparison of core body temperature between mice during Baseline 1 (21 °C; yellow), Test 1 (21 °C; light blue) and Cold 1 (4 °C; dark blue) at **c**, hour 2 **d**, hour 4 **e**, hour 6 and **f**, total time averaged in metabolic cages. **g** Time plot of the change in core body temperature between mice during Baseline 1 (21 °C; yellow), Test 1 (21 °C; light blue) and Cold 1 (4 °C; dark blue) normalized to the average core body temperature on BL1. Time plot of the change in core body temperature between mice during Baseline 1 (21 °C; yellow) and Test 1 (21 °C; light blue) during **h**, the total 2 h **i**, the total 4 h and **j**, total time averaged in metabolic cages. **b**-**j** Data shown as mean ± SEM, $n = 4$ mice per group. **c**-**f**, Repeated measures ANOVA. **h**-**j**, Paired *t*-test. *p < 0.05, **p < 0.01, ****p < 0.0001. h, hour; BL1, baseline 1; CL1, Cold 1; T1, Test 1. Schematics in **a** created with BioRender (https://biorender.com).

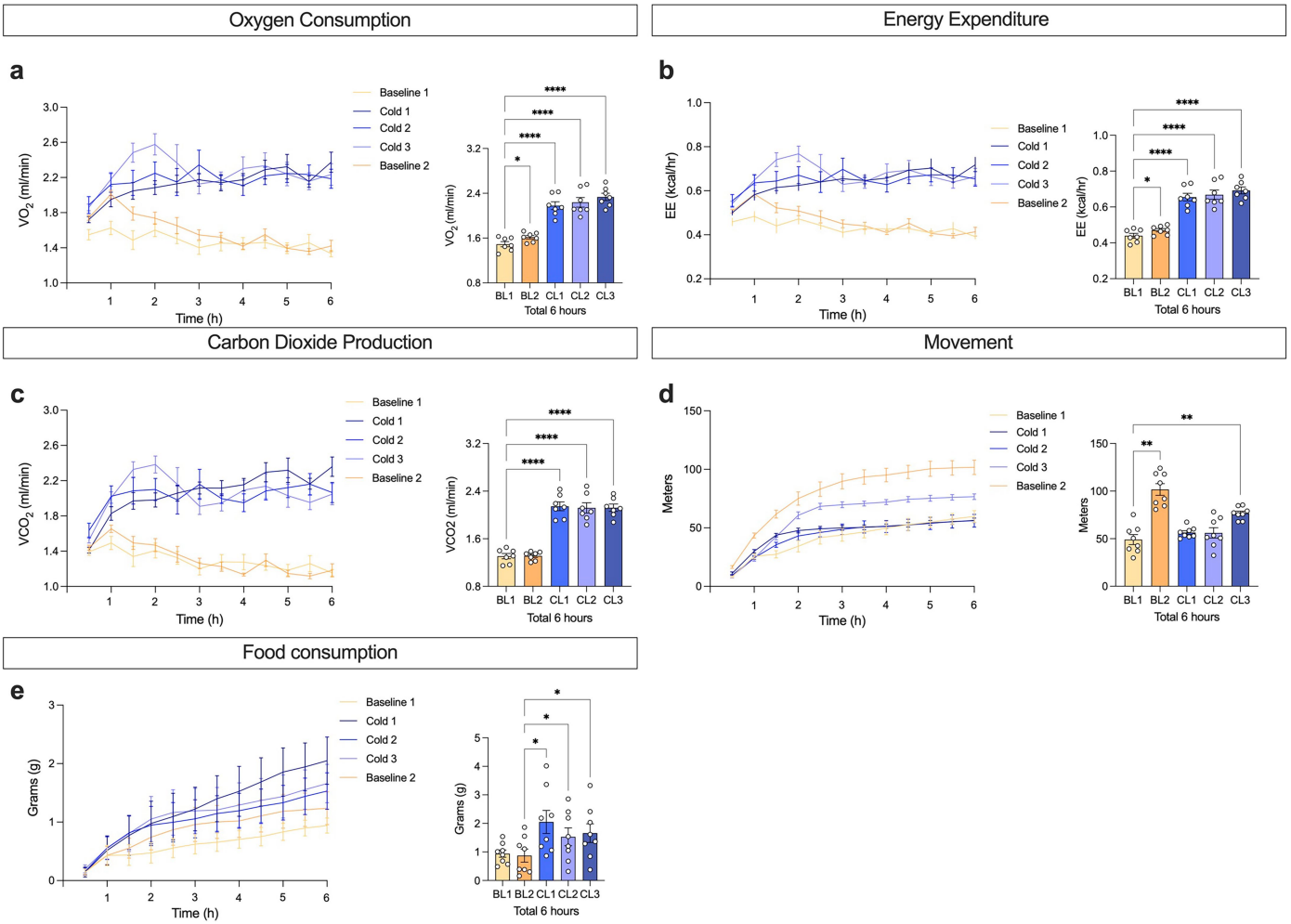

Extended Data Fig. 2 | Cold exposure increases metabolic rate and alters behavior. a Time plot of oxygen consumption between mice during Baseline 1 (21 °C; yellow), Baseline 2 (21 °C; orange), Cold 1 (4 °C; dark blue), Cold 2 (4 °C; blue), and Cold 3 (4 °C; light blue; left), with comparisons of total time averaged in metabolic cages (right). **b** Time plot of energy expenditure between mice during Baseline 1 (21 °C; yellow), Baseline 2 (21 °C; orange), Cold 1 (4 °C; dark blue), Cold 2 (4 °C; blue), and Cold 3 (4 °C; light blue; left), with comparisons of total time averaged in metabolic cages (right). **c** Time plot of carbon dioxide production between mice during Baseline 1 (21 °C; yellow), Baseline 2 (21 °C; orange), Cold 1 (4 °C; dark blue), Cold 2 (4 °C; blue), and Cold 3 (4 °C; light blue; left), with comparisons of total time averaged in metabolic cages (right). **d** Time plot of movement between mice during Baseline 1 (21 °C; yellow), Baseline 2 (21 °C; orange), Cold 1 (4 °C; dark blue), Cold 2 (4 °C; blue), and Cold 3 (4 °C; light blue; left), with comparisons of total time averaged in metabolic cages (right). **e** Time plot of food consumption between mice during Baseline 1 (21 °C; yellow), Baseline 2 (21 °C; orange), Cold 1 (4 °C; dark blue), Cold 2 (4 °C; blue), and Cold 3 (4 °C; light blue; left), with comparisons of total time averaged in metabolic cages (right). **a-e** Data shown as mean ± SEM, $n = 7$-8 mice per group. **a-e**, Repeated measures ANOVA. *p < 0.05, **p < 0.01, ***p < 0.001, ****p < 0.0001. BL1, baseline 1; BL2, baseline 2; CL1, cold 1; CL2, cold 2; CL3, cold 3; VO_2, oxygen consumption; VCO_2, carbon dioxide emission; h, hour; g, grams.

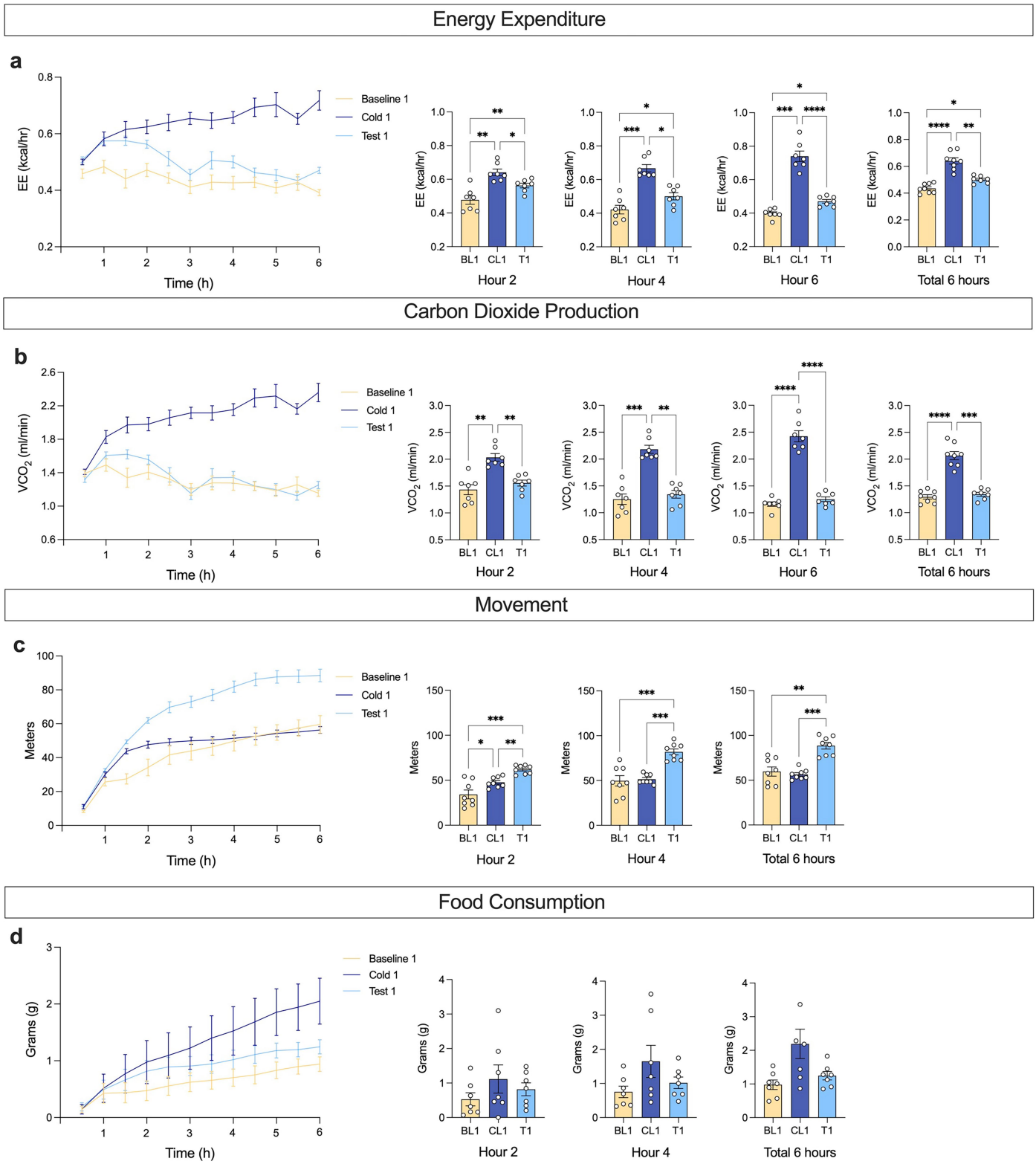

Extended Data Fig. 3 | A memory of a cold-paired context is sufficient to increase metabolic rate and alter behavior. a Time plot of energy expenditure between mice during Baseline 1 (21 °C; yellow), Test 1 (21 °C; light blue) and Cold 1 (4 °C; dark blue; left), with comparisons at hour 2, hour 4, hour 6 and total time averaged in metabolic cages (right). **b** Time plot of carbon dioxide production between mice during Baseline 1 (21 °C; yellow), Test 1 (21 °C; light blue) and Cold 1 (4 °C; dark blue; left), with comparisons at hour 2, hour 4, hour 6 and total time averaged in metabolic cages (right). **c** Time plot of movement between mice during Baseline 1 (21 °C; yellow), Test 1 (21 °C; light blue) and Cold 1 (4 °C; dark blue; left), with comparisons at hour 2, hour 4 and total time averaged in metabolic cages (right). **d** Time plot of food consumption between mice during Baseline 1 (21 °C; yellow), Test 1 (21 °C; light blue) and Cold 1 (4 °C; dark blue; left), with comparisons at hour 2, hour 4 and total time averaged in metabolic cages (right). **a-d** Data shown as mean ± SEM, $n = 7$-8 mice per group. **a-d**, Repeated measures ANOVA. *$p < 0.05$, **$p < 0.01$, ***$p < 0.001$, ****$p < 0.0001$. BL1, baseline 1; T1, Test 1; CL1, cold 1; VCO_2, carbon dioxide emission; EE; energy expenditure; h, hour.

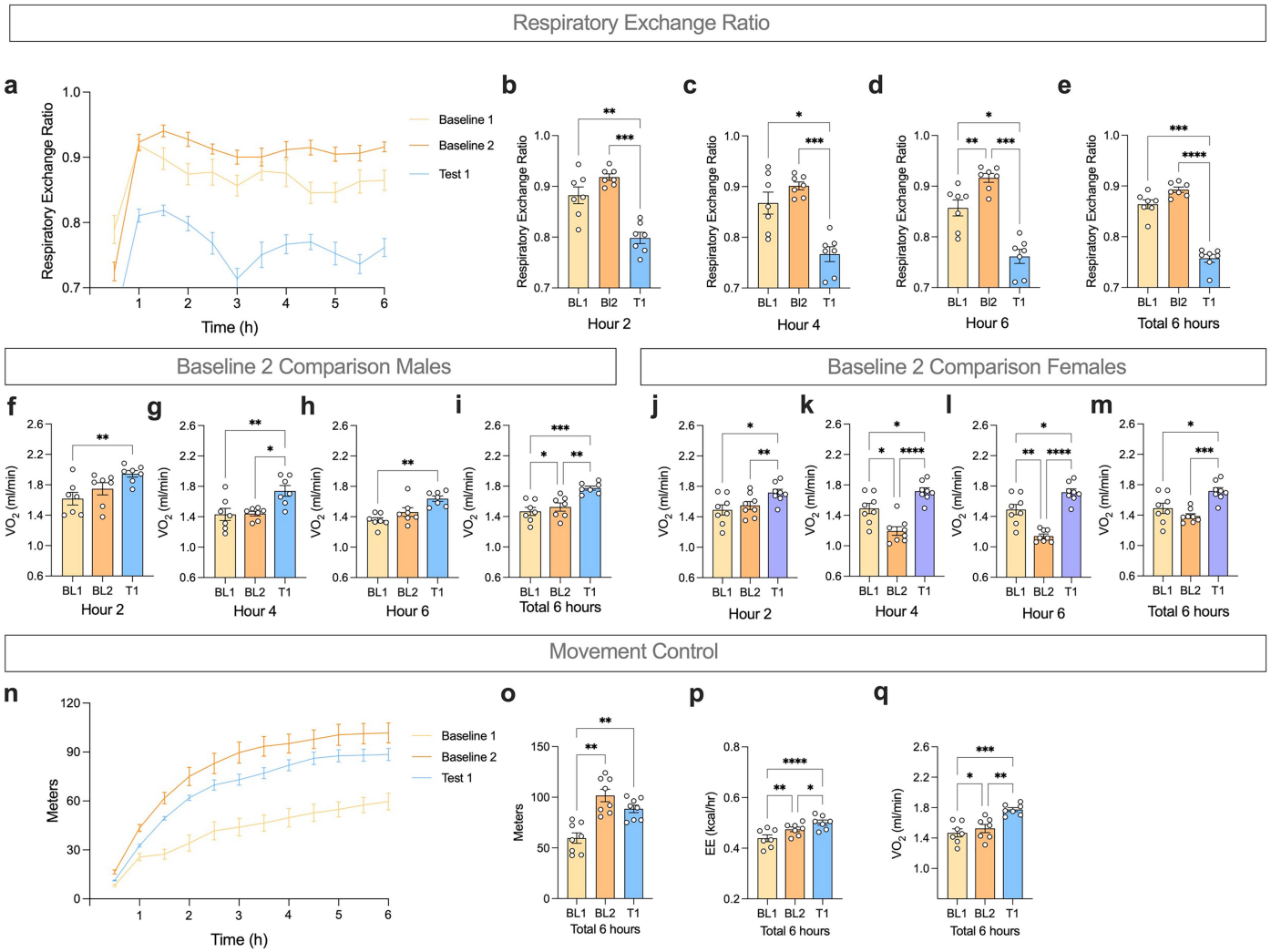

Extended Data Fig. 4 | Increases in metabolic rate on T1 compared to BL1 and BL2 is not due to activity. a Time plot of the respiratory exchange ratio between mice during BL1 (21 °C; yellow), BL2 (21 °C; orange) and T1 (21 °C; light blue). Comparison of the respiratory exchange ratio between mice during BL1 (21 °C; yellow), BL2 (21 °C; orange) and T1 (21 °C; light blue) at **b**, hour 2 **c**, hour 4 **d**, hour 6 and **e**, total time averaged in metabolic cages. Comparison of oxygen consumption between male mice during BL1 (21 °C; yellow), BL2 (21 °C; orange) and T1 (21 °C; light blue) at **f**, hour 2 **g**, hour 4 **h**, hour 6 and **i**, total time averaged in metabolic cages. Comparison of oxygen consumption between female mice during BL1 (21 °C; yellow), BL2 (21 °C; orange) and T1 (21 °C; light blue) at **j**, hour 2 **k**, hour 4 **l**, hour 6 and **m**, total time averaged in metabolic cages. **n** Time plot of movement between mice during BL1 (21 °C; yellow), BL2 (21 °C; orange) and T1 (21 °C; light blue). **o** Comparison of movement between mice during BL1 (21 °C; yellow), BL2 (21 °C; orange) and T1 (21 °C; light blue) for the total time averaged in metabolic cages. **p** Comparison of energy expenditure between mice during BL1 (21 °C; yellow), BL2 (21 °C; orange) and T1 (21 °C; light blue) for the total time averaged in metabolic cages. **q** Comparison of oxygen consumption between mice during BL1 (21 °C; yellow), BL2 (21 °C; orange) and T1 (21 °C; light blue) for the total time averaged in metabolic cages. **a-q** Data shown as mean ± SEM, $n = 7$-8 mice per group. **b-m**, **o-q**, Repeated measures ANOVA. *p < 0.05, **p < 0.01, ***p < 0.001, ****p < 0.0001. BL1, baseline 1; BL2, baseline 2; T1, Test 1; EE, energy expenditure; VO_2, oxygen consumption; h, hour.

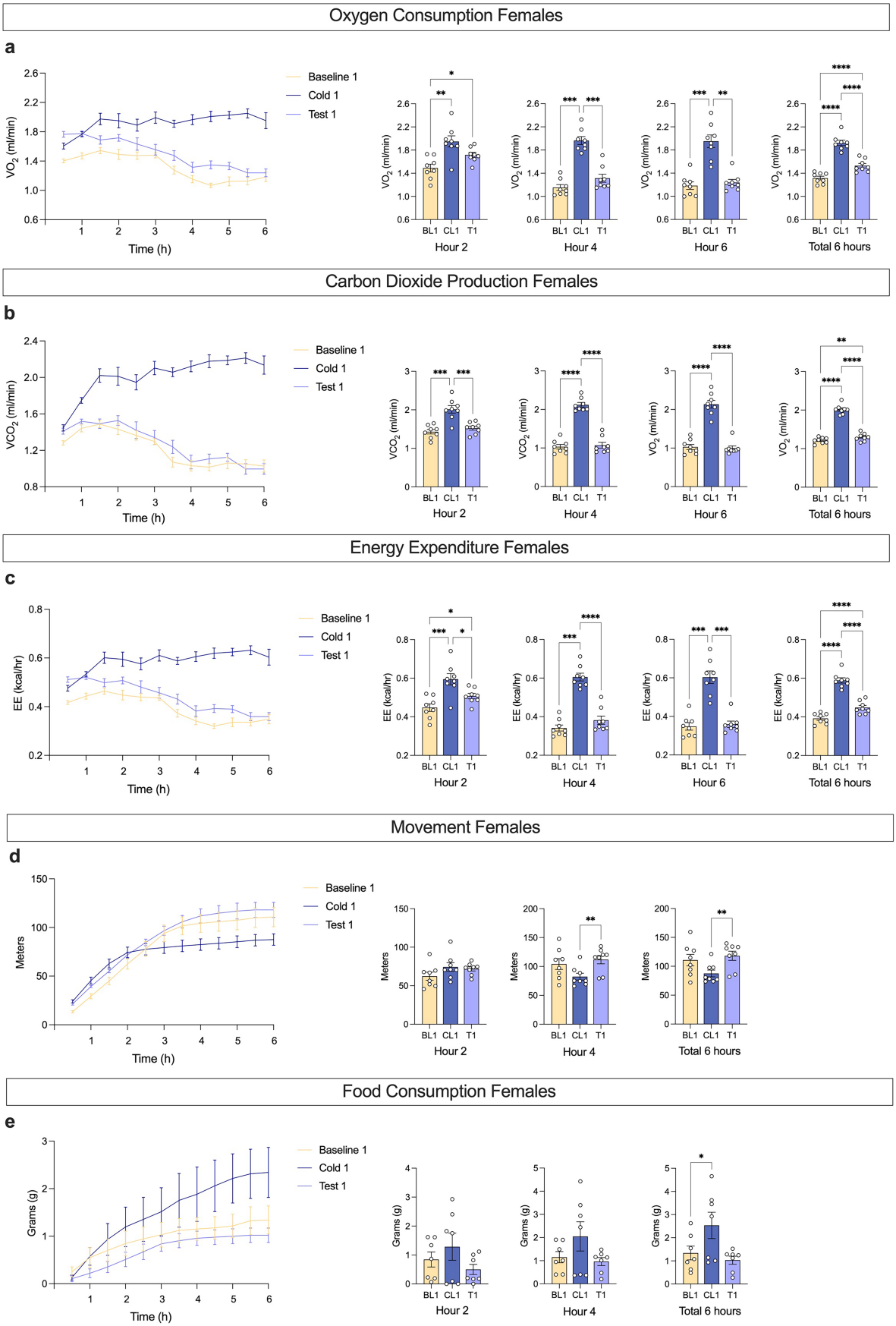

Extended Data Fig. 5 | See next page for caption.

Extended Data Fig. 5 | A memory of a cold-paired context is sufficient to increase metabolic rate and alter behavior in females. a Time plot of oxygen consumption between female mice during Baseline 1 (21 °C; yellow), Test 1 (21 °C; purple) and Cold 1 (4 °C; dark blue; left), with comparisons at hour 2, hour 4, hour 6 and total time averaged in metabolic cages (right). **b** Time plot of carbon dioxide production between female mice during Baseline 1 (21 °C; yellow), Test 1 (21 °C; purple) and Cold 1 (4 °C; dark blue; left), with comparisons at hour 2, hour 4, hour 6 and total time averaged in metabolic cages (right). **c** Time plot of energy expenditure between female mice during Baseline 1 (21 °C; yellow), Test 1 (21 °C; purple) and Cold 1 (4 °C; dark blue; left), with comparisons at hour 2, hour 4, hour 6 and total time averaged in metabolic cages (right). **d** Time plot of movement between female mice during Baseline 1 (21 °C; yellow), Test 1 (21 °C; purple) and Cold 1 (4 °C; dark blue; left), with comparisons at hour 2, hour 4 and total time averaged in metabolic cages (right). **e** Time plot of food consumption between female mice during Baseline 1 (21 °C; yellow), Test 1 (21 °C; light blue) and Cold 1 (4 °C; dark blue; left), with comparisons at hour 2, hour 4 and total time averaged in metabolic cages (right). **a-e** Data shown as mean ± SEM, n = 7-8 mice per group. **a-e**, Repeated measures ANOVA. *p < 0.05, **p < 0.01, ***p < 0.001, ****p < 0.0001. BL1, baseline 1; T1, Test 1; CL1, cold 1; VO_2, oxygen consumption; VCO_2, carbon dioxide emission; EE; energy expenditure; h, hour.

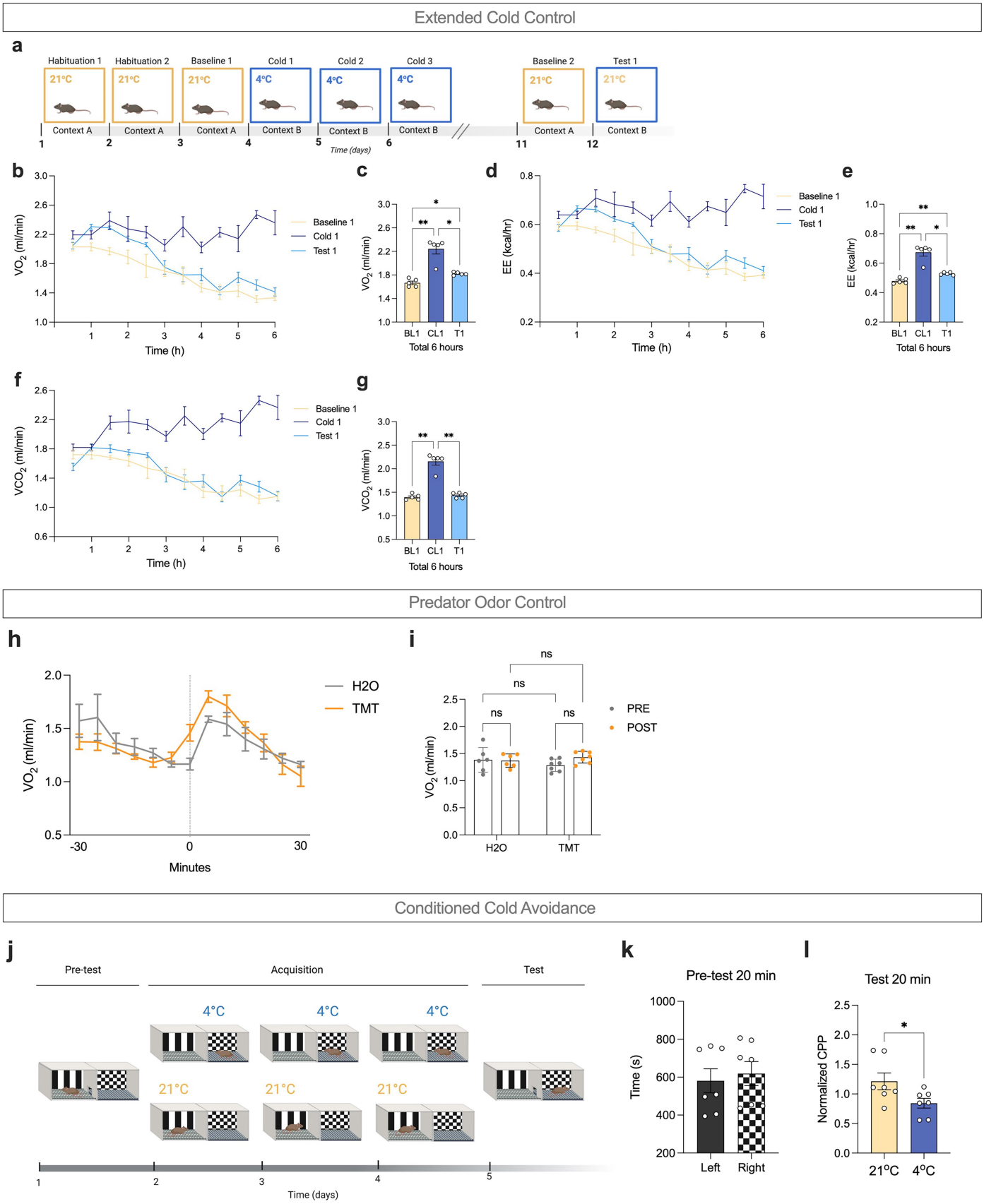

Extended Data Fig. 6 | See next page for caption.

Extended Data Fig. 6 | A cold memory is maintained after a prolonged break, is not due to stress, and causes avoidance behavior. a Diagrammatic representation of experimental timeline for Pavlovian conditioning to a cold-paired context with an extended (4 day) break **b** Time plot of oxygen consumption between mice during BL1 (21 °C; yellow), T1 (21 °C; light blue) and CL1 (4 °C; dark blue) following an extended (4 day) break, with **c** comparisons of total time averaged in metabolic cages (right). **d** Time plot of energy expenditure between mice during BL1 (21 °C; yellow), T1 (21 °C; light blue) and CL1 (4 °C; dark blue) following an extended (4 day) break, with **e** comparisons of total time averaged in metabolic cages (right). **f** Time plot of carbon dioxide production between mice during BL1 (21 °C; yellow), T1 (21 °C; light blue) and CL1 (4 °C; dark blue) following an extended (4 day) break, with **g** comparisons of total time averaged in metabolic cages (right). **h** Time plot of oxygen consumption between mice exposed to TMT (orange) or control mice exposed to H_2O (grey). **i** Comparison of pre (grey) and post (orange) odor exposure between mice exposed to TMT and control mice exposed to H_2O. **j** Diagrammatic representation of experimental timeline for Pavlovian conditioning to the cold-paired side, or no cold paired side, of a CPP apparatus. **k** Time spent in each chamber of the CPP apparatus during pre-test. **l** Place preference for the no cold paired side (yellow) of the CPP apparatus compared to the cold-paired side (blue), time spent in either the cold-paired side, or no cold paired side was divided by the time spent in the same chamber during pre-test (Test/Pre-test). **b-l,k,l**, Data shown as mean ± SEM, $n = 5$-7 mice per group. **c,e,g**, Repeated measures ANOVA, **i**, Two-way ANOVA, **k,l**, Unpaired *t*-test. *$p < 0.05$, **$p < 0.01$. BL1, baseline 1; T1, Test 1; CL1, cold 1; VO_2, oxygen consumption; VCO_2, carbon dioxide emission; h, hour; TMT, trimethylthiazoline; s, seconds; CPP, conditioned place preference. Schematics in **a** and **j** created with BioRender (https://biorender.com).

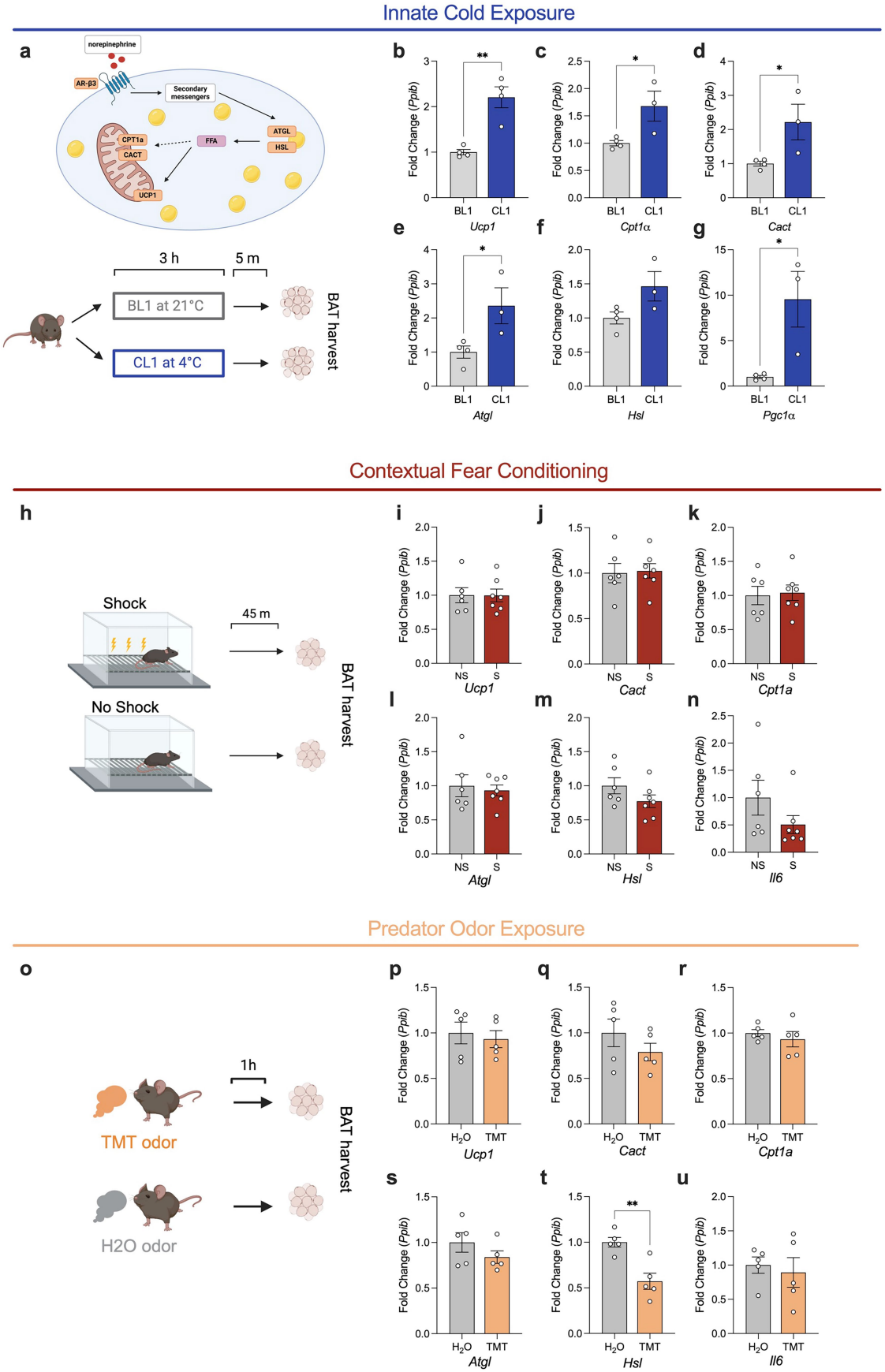

Extended Data Fig. 7 | See next page for caption.

Extended Data Fig. 7 | Innate cold exposure, but not stress, increases lipolytic and thermogenic gene expression in BAT. a Diagrammatic representation of the thermogenic pathway in BAT (above), with experimental timeline for tissue collection (below). Relative expression of lipolysis and thermogenesis genes **b**, *Ucp1*, **c**, *Cpt1α*, **d**, *Cact*, **e**, *Atgl*, **f**, *Hsl* and **g**, *Pgc1α* from the BAT of mice housed during BL1 (grey) compared cold exposed mice (CL1; blue). **h**, Diagrammatic representation of experimental timeline for tissue collection. Relative expression of lipolysis and thermogenesis genes **i**, *Ucp1*, **j**, *Cact*, **k**, *Cpt1α*, **l**, *Atgl*, **m**, *Hsl* and **n**, *Il6* from the BAT of mice that received foot shocks compared to no shock controls. n = 6-7 mice per group. **o** Diagrammatic representation of experimental timeline for tissue collection. Relative expression of lipolysis and thermogenesis genes **p**, *Ucp1*, **q**, *Cact*, **r**, *Cpt1α*, **s**, *Atgl*, **t**, *Hsl* and **u**, *Il6* from the BAT of mice that were exposed to TMT and H_2O exposed controls. **b-g**,**i-n**,**p-u**, Data shown as mean ± SEM n = 3-7 mice per group. **b-g**,**i-n**,**p-u**, unpaired t-test. *p < 0.05, **p < 0.01. BAT, brown adipose tissue; FFA, free fatty acid; BL1, baseline 1; CL1, cold 1; m, minutes; NS, no shock; S, shocked; TMT, trimethylthiazoline; h, hour. Schematics in **a**, **h** and **o** created with BioRender (https://biorender.com).

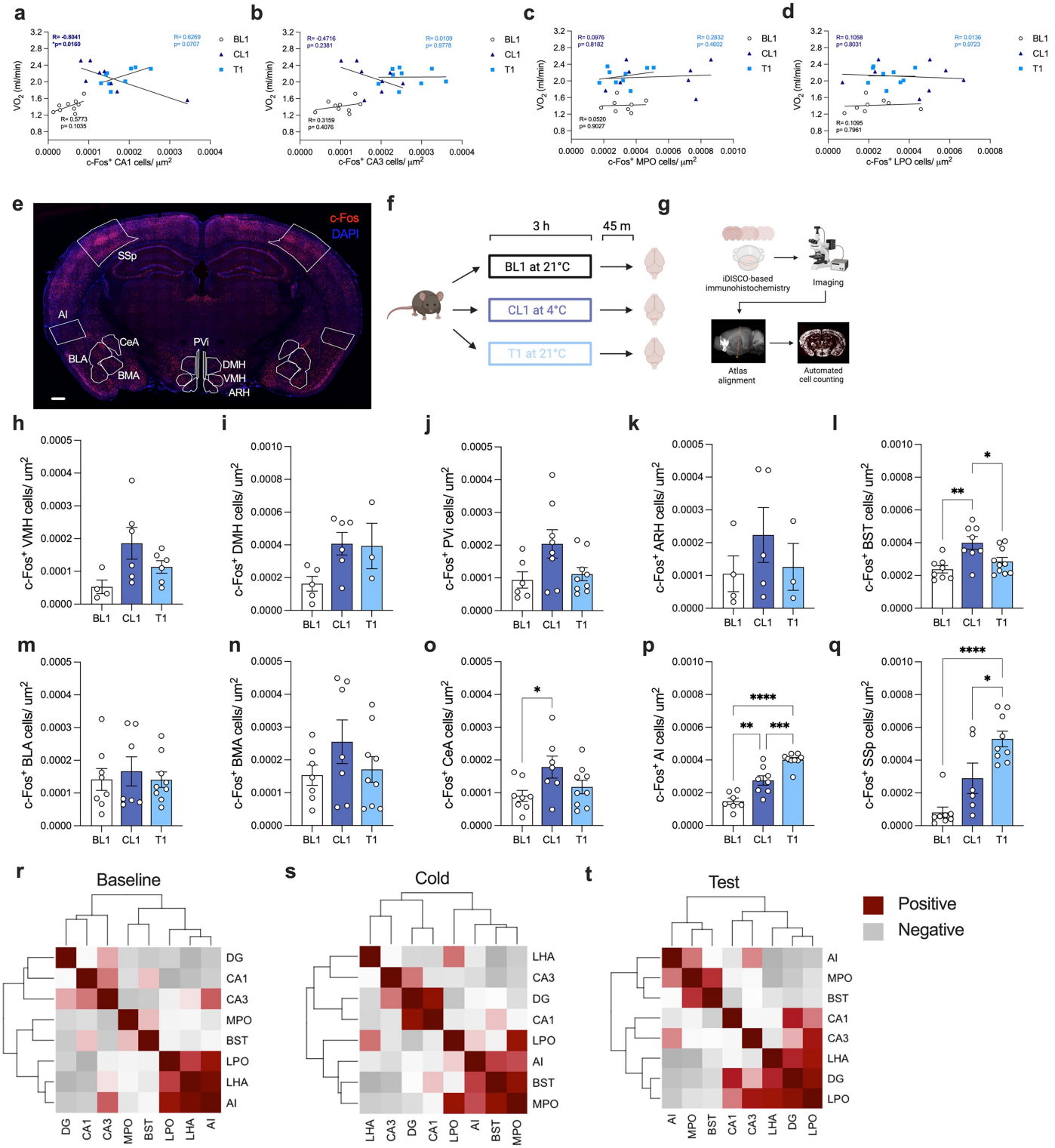

Extended Data Fig. 8 | See next page for caption.

Extended Data Fig. 8 | Retrieval of a cold memory does not correlate metabolism with Fos$^+$ in CA3, MPO or LPO, or increase neural activity in every region. Correlation between oxygen consumption and Fos$^+$ cells in **a**, CA1, **b**, CA3, **c**, MPO, and **d**, LPO between mice during BL1 (white), CL1 (dark blue) and T1 (light blue). **e** Representative image of hippocampal slice with Fos$^+$ cells (red) and DAPI$^+$ cells (blue). **f** Experimental timeline for tissue collection. **g** Diagrammatic representation of the automated brain-wide Fos detection pipeline used to identify Fos$^+$ cells in multiple brain regions simultaneously. Comparison of Fos$^+$ neurons normalized to area in the **h**, VMH **i**, DMH **j**, PVi **k**, ARH **l**, BST **m**, BLA **n**, BMA **o**, CeA **p**, AI and **q**, SSp between mice housed during BL1 (white), CL1 (dark blue) and T1 (light blue). Correlation matrix of Fos$^+$ cells normalized to area during **r**, baseline day (BL1), **s**, cold training day (CL1) and **t**, the recall of a contextual cold memory on test day, with positive (red) and negative (grey) correlations. **h-t**, Data shown as mean ± SEM, **a-d, h-t** n = 3-9 mice per group. **a-d**, Simple linear regression with slope comparison, **h-q**, One-way ANOVA. *p < 0.05, **p < 0.01, ***p < 0.001, ****p < 0.0001. BL1, baseline 1; T1, Test 1; CL1, cold 1; CA3, cornu ammonis 3; CA1, cornu ammonis 1; VO_2, oxygen consumption; MPO, medial preoptic area; LPO, lateral preoptic area. BL1, baseline 1; T1, Test 1; CL1, cold 1; VMH, ventromedial hypothalamic nucleus; DMH, dorsomedial nucleus of the hypothalamus; AI, agranular insular area; SSp, primary somatosensory area; PVi, periventricular hypothalamic nucleus -intermediate part; ARH, arcuate hypothalamic nucleus; BST, bed nuclei of the stria terminalis; BLA, basolateral amygdalar nucleus; BMA, basomedial amygdalar nucleus; CeA; central amygdalar nucleus; DG, dentate gyrus; CA3, cornu ammonis 3; CA1, cornu ammonis 1; LHA, lateral hypothalamic area. Schematics in **f** and **g** created with BioRender (https://biorender.com).

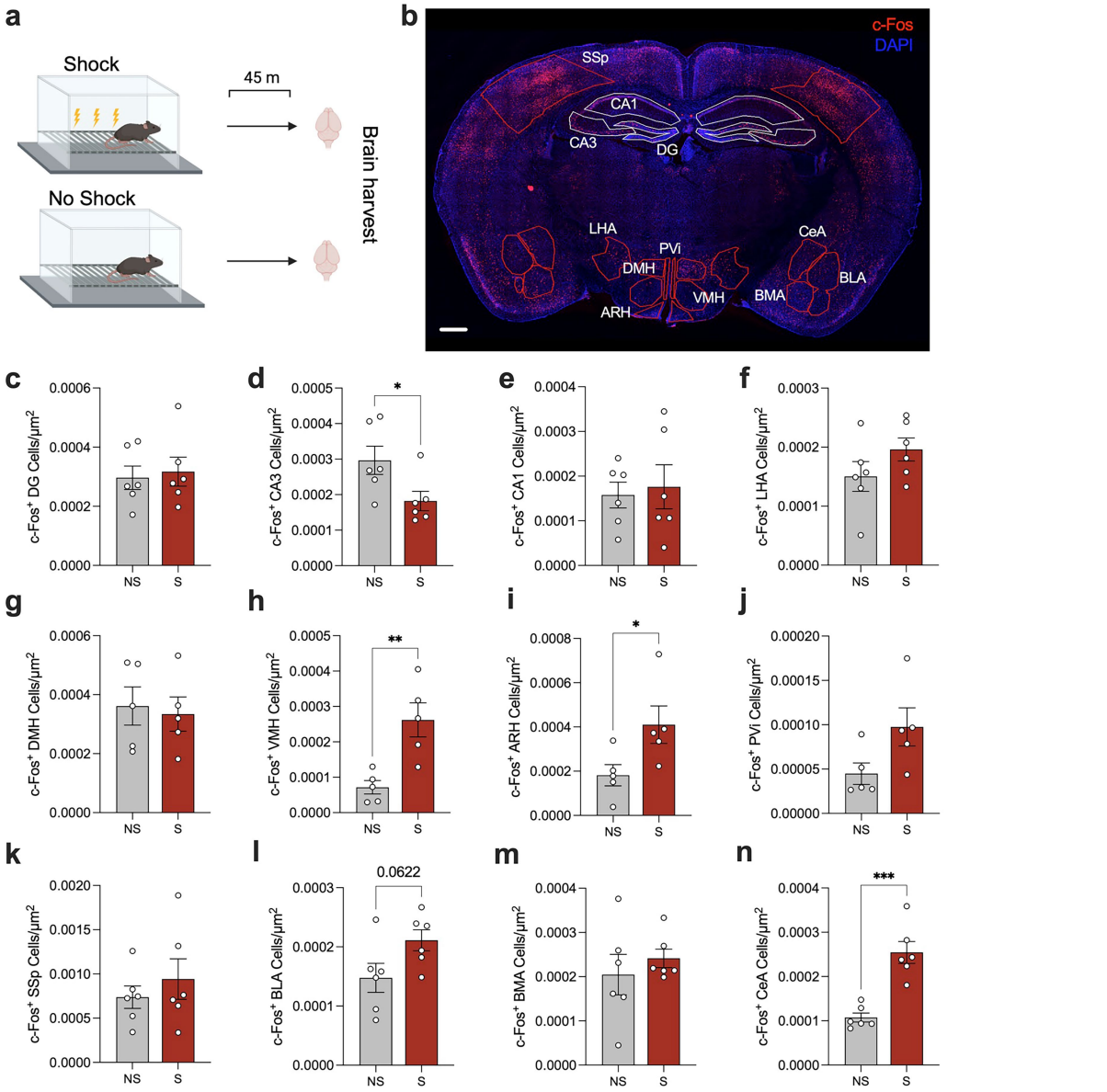

Extended Data Fig. 9 | Distinct stress-related stimuli activate divergent brain regions. a Diagrammatic representation of experimental timeline for tissue collection. **b** Representative image of hippocampal slice with Fos$^+$ cells (red) and DAPI$^+$ cells (blue). Comparison of Fos$^+$ neurons normalized to area in the **c**, DG **d**, CA3 **e**, CA1 **f**, LHA **g**, DMH **h**, VMH **i**, ARH **j**, PVi **k**, SSp **l**, BLA **m**, BMA and **n**, CeA of mice that received foot shocks (red) compared to no shock controls (grey). Data shown as mean ± SEM, **c-n**, $n = 5$-6 mice per group. **c-n**, unpaired *t*-test. *p < 0.05, **p < 0.01, ***p < 0.001. S, shocked; NS, no shock; DG, dentate gyrus; CA3, cornu ammonis 3; CA1, cornu ammonis 1; LHA, lateral hypothalamic area; DMH, dorsomedial nucleus of the hypothalamus; VMH, ventromedial hypothalamic nucleus; ARH, arcuate hypothalamic nucleus; PVi, periventricular hypothalamic nucleus-intermediate part; SSp, primary somatosensory area; BLA, basolateral amygdalar nucleus; BMA, basomedial amygdalar nucleus; CeA; central amygdalar nucleus. Schematic in **a** created with BioRender (https://biorender.com).

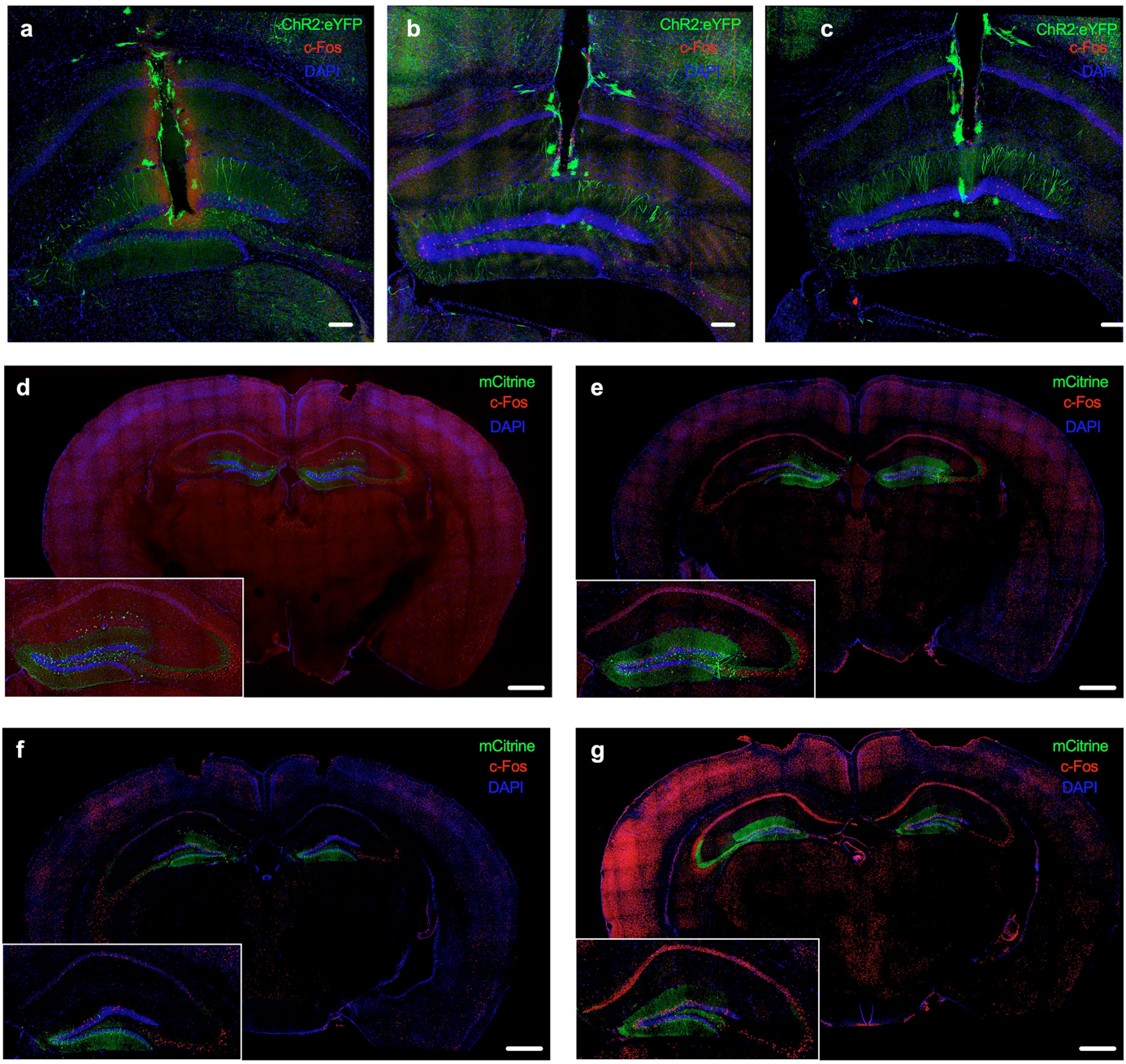

Extended Data Fig. 10 | Representative images of optogenetic and chemogenetic experiments. a-c Representative images of hippocampal slices with Fos$^+$ cells (red), ChR2$^+$ cells (green), DAPI$^+$ cells (blue) and optogenetic implant tracts. **d-g** Representative images of hippocampal slices with Fos$^+$ cells (red), mCitrine$^+$ cells (green) and DAPI$^+$ cells (blue) of chemogenetic experiments.

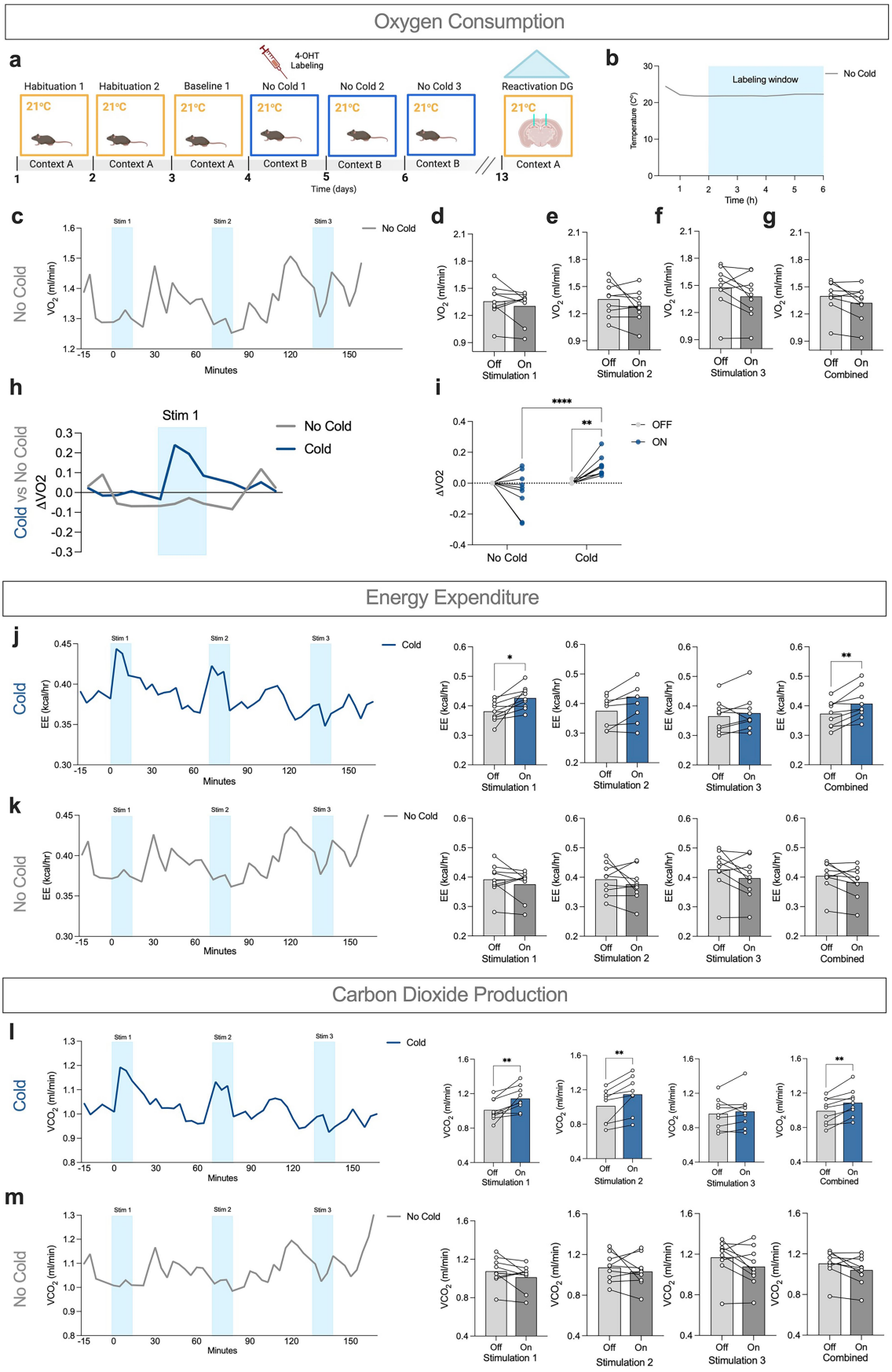

Extended Data Fig. 11 | See next page for caption.

Extended Data Fig. 11 | Artificial reactivation of cold-sensitive memory engrams in the DG increases metabolic rate. a Experimental timeline to label and reactivate no cold engrams. **b** Environmental temperature during the labeling window on no cold day 1. **c** Time plot of oxygen consumption during artificial reactivation of no cold control engrams (Blue bars indicate laser activation). **d, e, f** Comparison of oxygen consumption between the on (dark grey) and off (light grey) epochs during the three stimulations of no cold control cells, with **g**, all stimulations combined. **h** Change of oxygen consumption before, during and after stimulating cold-sensitive engram cells (blue) and no cold control cells (grey) normalized to the initial 20 min of recording. **i** Comparison of the change in oxygen consumption during on (blue) and off (grey) epochs between cold-sensitive stimulated cells and no cold control stimulated cells. Time plot of energy expenditure during artificial reactivation of **j**, cold-sensitive engrams (left) and **k**, no cold control cells (left), with comparison of oxygen consumption between the on (blue) and off (grey) epochs during the three stimulations of cold-sensitive cells (right). Time plot of carbon dioxide production during artificial reactivation of **l**, cold-sensitive engrams (left) and **m**, no cold control cells (left), with comparison of oxygen consumption between the on (blue) and off (grey) epochs during the three stimulations of cold-sensitive cells (right). Blue bars indicate the time the laser was turned on during the 3 stimulation periods. **d-g,i-m**, Data shown as mean, **c-m**, $n = 8$-9 mice per group. **d-g,j-m**, paired *t*-test, **i**, two-way ANOVA. *$p < 0.05$, **$p < 0.01$, ****$p < 0.0001$. VCO_2, carbon dioxide production; Stim 1, stimulation 1; Stim 2, stimulation 2; Stim 3, stimulation 3. Schematics in **a** created with BioRender (https://biorender.com).

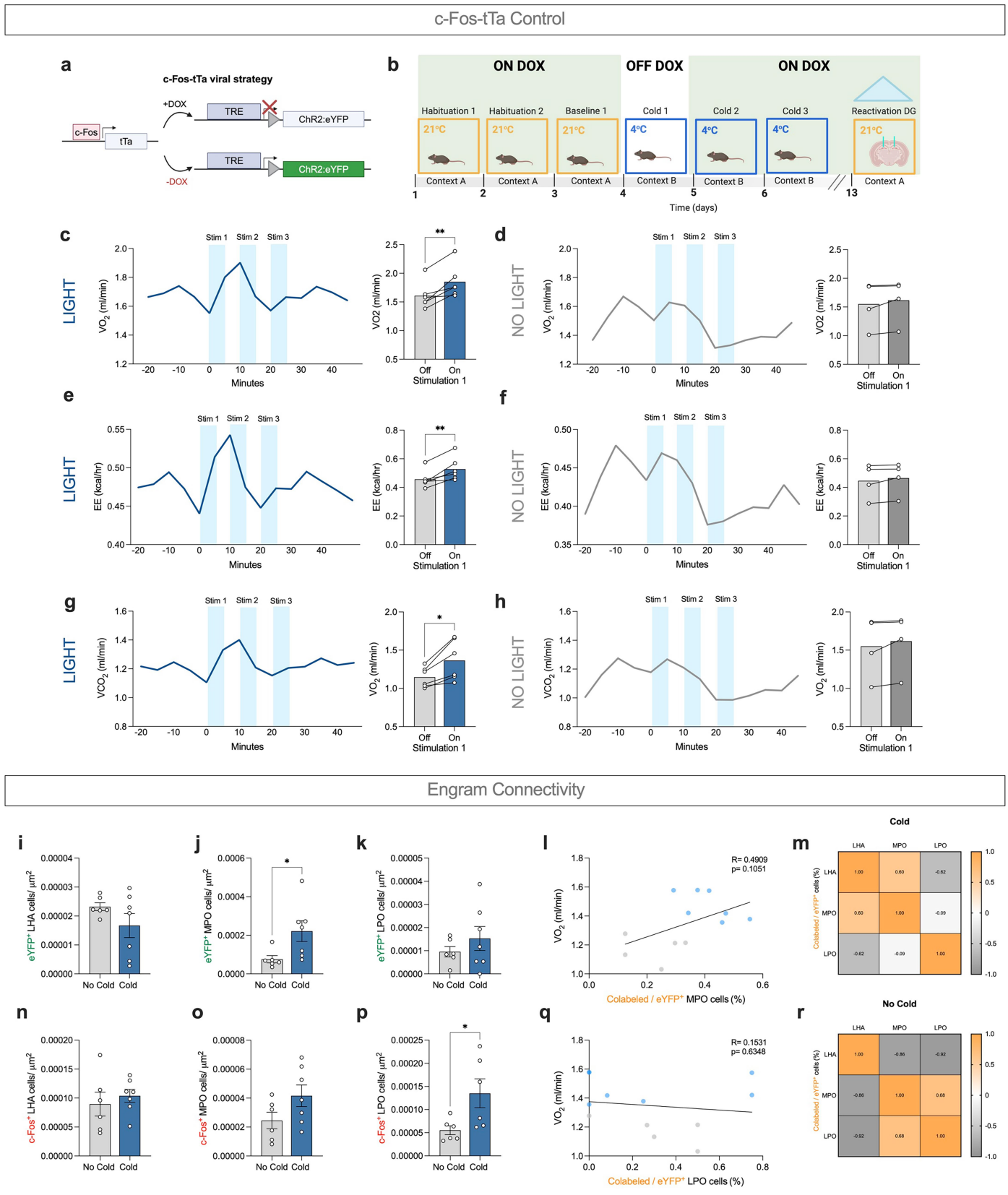

Extended Data Fig. 12 | See next page for caption.

Extended Data Fig. 12 | Artificial reactivation of cold-sensitive memory engrams in the DG increases metabolic rate in Fos tTA mice and engram activity in the hypothalmus. a Diagrammatic representation of the Fos tTA transgenic labeling system for ChR2::GFP expression and **b**, timeline to label cold-sensitive engrams woth Fos tTA mice. Time plot of **c**, oxygen consumption **e**, energy expenditure and **g**, carbon dioxide production during artificial reactivation of cold-sensitive engrams (left), with comparison of on (blue) and off (grey) epochs during the first stimulation of cold-sensitive cells (right). Time plot of **d**, oxygen consumption **f**, energy expenditure and **h**, carbon dioxide production during artificial reactivation of no cold control cells (left), with comparison of on (blue) and off (grey) epochs during the first stimulation of no cold control cells (right). Comparison of $eYFP^+$ neurons normalized to area between the cold stimulated (dark blue) and no-cold stimulated (grey) cohorts in **i**, the LHA, **j**, the MPO and **k**, the LPO. Comparison of Fos^+ neurons normalized to area between the cold stimulated (dark blue) and no-cold stimulated (grey) cohorts in **n**, the LHA, **o**, the MPO and **p**, the LPO. Correlation between the percentage of colabeled/$eYFP^+$ cells in **i**, the MPO and **q**, the LPO with oxygen consumption after cold stimulation (blue) and no-cold stimulation (grey). Correlation of percentage of colabeled/$eYFP^+$ cells between regions after optogenetic stimulation of **m**, cold-sensitive engrams and **r**, no-cold engrams. Blue bars indicate the time the laser was turned on during the 3 stimulation periods. **a-h**, Data show as mean and, **i-k,n-p**, as mean ± SEM, $n = 6$-7 mice per group. **c-h,i-p**, unpaired *t*-test, **l,q**, simple linear regression. $^*p < 0.05$, $^{**}p < 0.01$. ChR2, channelrhodopsin-2; GFP, green fluorescent protein; DOX, doxycycline; VO_2, oxygen consumption; VCO_2, carbon dioxide production; Stim 1, stimulation 1; Stim 2, stimulation 2; Stim 3, stimulation 3; LHA, lateral hypothalamic area; MPO, medial preoptic area; LPO, lateral preoptic area. Schematics in **a** and **b** created with BioRender (https://biorender.com).

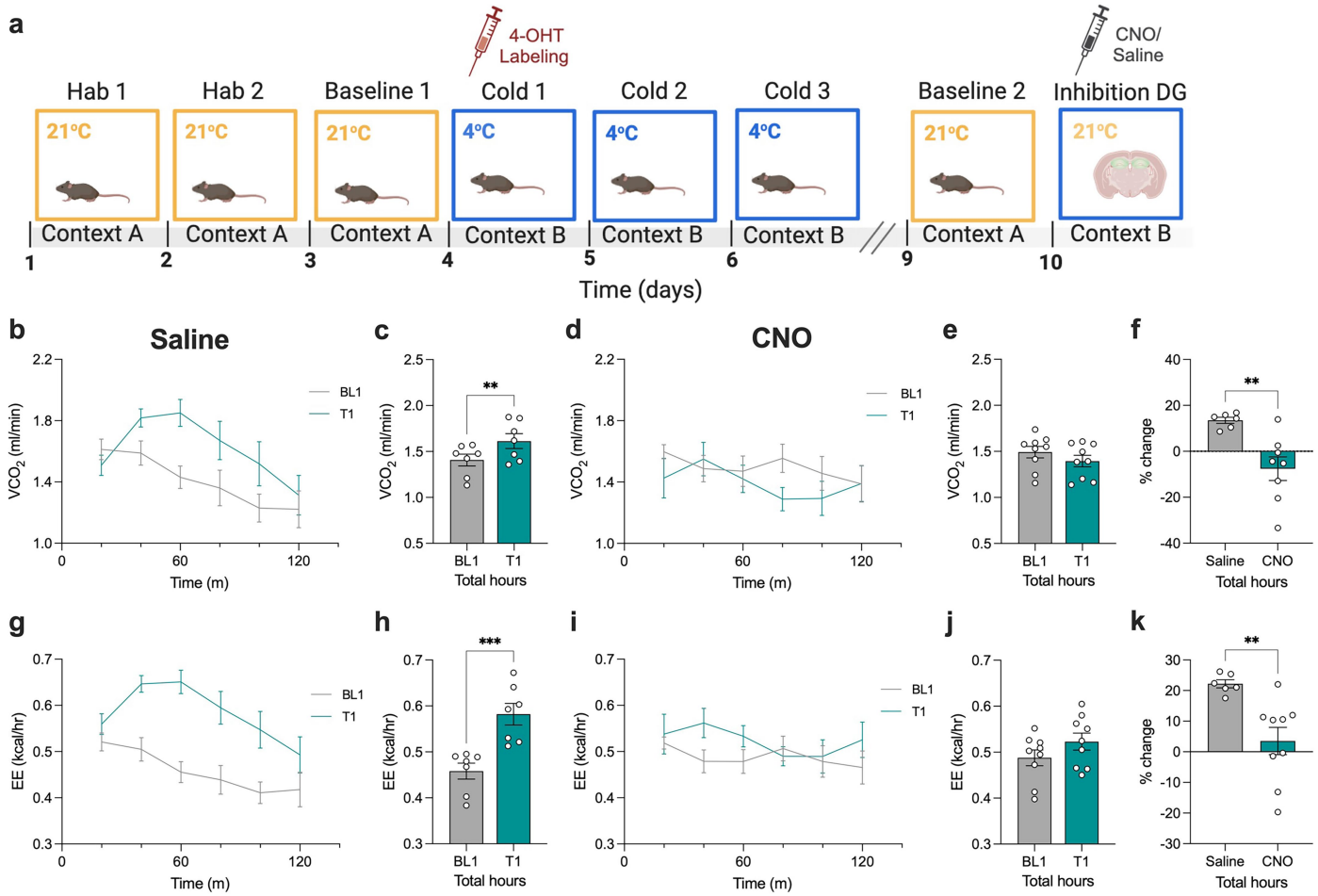

Extended Data Fig. 13 | Inhibition of cold-sensitive engrams prevents the memory associated increases in metabolic rates. a Diagrammatic representation of experimental timeline to label and chemogenetically inhibit contextual cold memory engrams. **b** Time plot of carbon dioxide production of saline injected mice during baseline 1 (grey) and test day 1 (teal), with **c**, the total time averaged. **d** Time plot of carbon dioxide production of CNO injected mice during baseline 1 (grey) and test day 1 (teal) with **e**, the total time averaged. **f** Comparison of the percentage change of carbon dioxide production between saline (grey) and CNO (teal) injected mice on test day 1. **g** Time plot of energy expenditure of saline injected mice during baseline 1 (grey) and test day 1 (teal) with **h**, the total time averaged. **i** Time plot of energy expenditure of CNO injected mice during baseline 1 (grey) and test day 1 (teal) with **j**, the total time averaged. **k** Comparison of the percentage change of energy expenditure between saline (grey) and CNO (teal) injected mice on test day 1. Data shown as mean ± SEM, **b-k**, $n = 7$-8 mice per group. **c,e,h,j**, paired *t*-test, **f,k**, unpaired *t*-test. $^{**}p < 0.01$, $^{***}p < 0.001$. 4-OHT, 4-hydroxytamoxifen; VCO_2, carbon dioxide emission; EE, energy expenditure; T1, test 1; BL1, baseline 1; m, minutes; CNO, clozapine N-oxide. Schematics in **a** created with BioRender (https://biorender.com).

nature portfolio

Corresponding author(s): Tomás Ryan

Last updated by author(s): Aug 23, 2024

Reporting Summary

Nature Portfolio wishes to improve the reproducibility of the work that we publish. This form provides structure for consistency and transparency in reporting. For further information on Nature Portfolio policies, see our Editorial Policies and the Editorial Policy Checklist.

Statistics

For all statistical analyses, confirm that the following items are present in the figure legend, table legend, main text, or Methods section.

n/a	Confirmed
☐	☒ The exact sample size (*n*) for each experimental group/condition, given as a discrete number and unit of measurement
☐	☒ A statement on whether measurements were taken from distinct samples or whether the same sample was measured repeatedly
☐	☒ The statistical test(s) used AND whether they are one- or two-sided *Only common tests should be described solely by name; describe more complex techniques in the Methods section.*
☐	☒ A description of all covariates tested
☐	☒ A description of any assumptions or corrections, such as tests of normality and adjustment for multiple comparisons
☐	☒ A full description of the statistical parameters including central tendency (e.g. means) or other basic estimates (e.g. regression coefficient) AND variation (e.g. standard deviation) or associated estimates of uncertainty (e.g. confidence intervals)
☐	☒ For null hypothesis testing, the test statistic (e.g. *F*, *t*, *r*) with confidence intervals, effect sizes, degrees of freedom and *P* value noted *Give P values as exact values whenever suitable.*
☒	☐ For Bayesian analysis, information on the choice of priors and Markov chain Monte Carlo settings
☒	☐ For hierarchical and complex designs, identification of the appropriate level for tests and full reporting of outcomes
☐	☒ Estimates of effect sizes (e.g. Cohen's *d*, Pearson's *r*), indicating how they were calculated

Our web collection on statistics for biologists contains articles on many of the points above.

Software and code

Policy information about availability of computer code

Data collection	Metabolic Cages (Promethion, Sable Systems), LAS X software.
Data analysis	NeuroInfo (MBF Bioscience), Rstudio, Fiji (ImageJ), Prism 10.

For manuscripts utilizing custom algorithms or software that are central to the research but not yet described in published literature, software must be made available to editors and reviewers. We strongly encourage code deposition in a community repository (e.g. GitHub). See the Nature Portfolio guidelines for submitting code & software for further information.

Data

Policy information about availability of data

All manuscripts must include a data availability statement. This statement should provide the following information, where applicable:

- Accession codes, unique identifiers, or web links for publicly available datasets
- A description of any restrictions on data availability
- For clinical datasets or third party data, please ensure that the statement adheres to our policy

In this study the Allen Brain Atlas was used as a reference for brain regions. This database is publicly available at https://mouse.brain-map.org/static/atlas. All data necessary for the interpretation and replication of the reported findings are contained within the manuscript and supplemental information. Raw data supporting the findings of this study are available from the corresponding author upon reasonable request. Statistical source data is provided with this paper. Detailed figure source data is also provided with this paper.

Research involving human participants, their data, or biological material

Policy information about studies with human participants or human data. See also policy information about sex, gender (identity/presentation), and sexual orientation and race, ethnicity and racism.

Reporting on sex and gender	N/A
Reporting on race, ethnicity, or other socially relevant groupings	N/A
Population characteristics	N/A
Recruitment	N/A
Ethics oversight	N/A

Note that full information on the approval of the study protocol must also be provided in the manuscript.

Field-specific reporting

Please select the one below that is the best fit for your research. If you are not sure, read the appropriate sections before making your selection.

☒ Life sciences ☐ Behavioural & social sciences ☐ Ecological, evolutionary & environmental sciences

For a reference copy of the document with all sections, see nature.com/documents/nr-reporting-summary-flat.pdf

Life sciences study design

All studies must disclose on these points even when the disclosure is negative.

Sample size	Sample sizes were estimated based on standards and credibility in the field of thermoregulation, and based on pilot metabolism data in response to real time cold exposure experiments in the research group of Lydia Lynch before conducting this study.
Data exclusions	Experiments that involved sterotactic surgery showed unsuccessful surgical targeting in under 5 % of cases, but those subjects were excluded from analysis based on histological validation. No other animals we excluded from any experiment in this study, and no extreme statistical outliers were observed for any experiment.
Replication	All of the core findings of this manuscript were reproduced by two to three different investigators in our group. All technical details have been reported so that these findings can easily be replicated in any other laboratory with similar apparatus. All experiments were replicated independently between 2 and 4 times.
Randomization	Animals were randomly allocated to experimental groups, and groups were counter-balanced for cage of origin.
Blinding	Investigators were blind to experimental groups at all points of data collection and analysis.

Reporting for specific materials, systems and methods

We require information from authors about some types of materials, experimental systems and methods used in many studies. Here, indicate whether each material, system or method listed is relevant to your study. If you are not sure if a list item applies to your research, read the appropriate section before selecting a response.

Materials & experimental systems

n/a	Involved in the study
☐	☒ Antibodies
☒	☐ Eukaryotic cell lines
☒	☐ Palaeontology and archaeology
☐	☒ Animals and other organisms
☒	☐ Clinical data
☒	☐ Dual use research of concern
☒	☐ Plants

Methods

n/a	Involved in the study
☒	☐ ChIP-seq
☒	☐ Flow cytometry
☒	☐ MRI-based neuroimaging

Antibodies

Antibodies used	Chicken polyclonal anti-GFP (ref# A10262, 1:1000, Invitrogen, Waltham, MA), Rabbit polyclonal IgG anti-c-Fos (ref# 226008, 1:1000, Invitrogen, Waltham, MA), Alexa 568 Anti-Rabbit IgG (ref# 11011, 1:500, Invitrogen, Waltham, MA) and Alexa 488 Anti-Chicken IgG (ref# A11039, 1:500, Invitrogen, Waltham, MA).
Validation	All antibodies were validated by the manufacturer as stated on their website. Moreover, antibody concentration was specifically validated for this study by comparing 1:1000 concentrations with 1:500 and 1:5000. The concentration that achieved optimal signal was selected.

Animals and other research organisms

Policy information about studies involving animals; ARRIVE guidelines recommended for reporting animal research, and Sex and Gender in Research

Laboratory animals	Mice, C57Bl/6j, 6 - 12 weeks of age.
Wild animals	No wild animals were used in this study.
Reporting on sex	The majority of the study was conducted using only male mice. Following revision, we have included one experiment with female mice, which explicitly tests the effect of sex on cold memory formation.
Field-collected samples	No field collected samples were used in this study
Ethics oversight	All animal work was performed in compliance with the Ryan and Lynch laboratory project licenses, with ethical approval from the Trinity College Dublin ethics committee, the Animal Research Ethics Committee from the Health Products Regulatory Authority (HPRA), the Brigham and Women's Hospital Institutional Animal Care and Use Committee guidelines.

Note that full information on the approval of the study protocol must also be provided in the manuscript.

Plants

Seed stocks	N/A
Novel plant genotypes	N/A
Authentication	N/A